

1 **Using ignimbrites to quantify structural relief growth and**
2 **understand deformation processes; implications for the**
3 **development of the Western Andean Slope, northernmost**
4 **Chile**

5

6 M.E. van Zalinge^{1,*}, R.S.J. Sparks¹, L.A. Evenstar¹, F.J. Cooper¹, J. Aslin¹, D.J.
7 Condon²

8

9 ¹ School of Earth Sciences, University of Bristol, Wills Memorial Building, Queens
10 Road, Clifton, Bristol, BS8 1RJ, United Kingdom

11 ² British Geological Survey, NERC Isotope Geosciences Facilities, Nicker Hill,
12 Keyworth, Nottingham, NG12 5GG, United Kingdom

13 * m.vanzalinge@bristol.ac.uk

14

15 **ABSTRACT**

16 Large volume ignimbrites are excellent spatial and temporal markers for local
17 deformation and structural relief growth, as they completely inundate and bury the
18 underlying palaeo-topography and leave planar surfaces with relatively uniform, low
19 gradient slopes dipping less than 2°. Using one of these planar surfaces as a reference
20 frame, we employ a line-balanced technique to reconstruct the original morphology of
21 an ignimbrite that has undergone post-emplacement deformation. This method allows
22 us to constrain both the amount of post-eruptive deformation and the topography of
23 the pre-eruptive palaeo-landscape. Our test case is the unwelded surface of the 21.9
24 Ma Cardones ignimbrite located on the Western Andean Slope of the Central Andes
25 in northernmost Chile (18°20'S). By reconstructing the original surface slope of this
26 ignimbrite, we demonstrate that the pre-21.9 Ma topography of the Western Andean
27 Slope was characterised by structural relief growth and erosion in the east, and the
28 creation of accommodation space and sedimentation in the west. The palaeo-slope at
29 this time was dissected by 450 ± 150 m-deep river valleys that accumulated great
30 thicknesses (>1000 m) of the Cardones ignimbrite, and likely controlled the location
31 of the present-day Lluta Quebrada as a result of differential welding compaction of
32 the ignimbrite. Our reconstruction suggests that growth of the Western Andean Slope
33 had already started by ca. 23 Ma, consistent with slow and steady models for uplift of
34 the Central Andes. Subsequent deformation in the Miocene generated up to $1725 \pm$
35 165 m of structural relief, of which more than 90% can be attributed to fault-related
36 folding of the ca. 40 km-wide Huaylillas Anticline. Uplift related to regional forearc
37 tilting is less than 10% and could have been zero. The main phase of folding likely
38 occurred in the mid-to-late Miocene and had ceased by ca. 6 Ma.

39

40 **INTRODUCTION**

41 Subduction-related ignimbrite flare-ups, typically lasting for several million years,
42 have occurred in the Great Basin, USA and the Central Andes, South America during
43 the Cenozoic (e.g. De Silva, 1989; Best et al., 2009). During these flare-ups, large
44 magnitude eruptions produced ignimbrites with individual volumes of a few hundred
45 to a few thousand cubic kilometres. Ignimbrites can cover areas of thousands of
46 square kilometres, changing the landscape dramatically. The thickness of an
47 ignimbrite is controlled by the total volume erupted, discharge rate and flow velocity
48 of the pyroclastic flow, as well as the underlying topography. In general, thicker
49 deposits are found in valleys and depressions, while thinner deposits occur on
50 topographic highs (e.g. Walker et al., 1980; Wright et al., 1980; Walker, 1983; Wilson
51 and Hildreth, 1997; Henry and Faulds, 2010; Cas et al. 2011; Roche et al. 2016). The
52 largest ignimbrites can completely inundate and bury the topography, leaving planar
53 regional ignimbrite surfaces with very low slopes (e.g. Walker, 1983). Consequently,
54 these ignimbrite surfaces make excellent spatial and temporal palaeo-markers for
55 recording deformation. By applying a line-balanced reconstruction technique to the
56 top surface of an ignimbrite, we demonstrate that it is possible to constrain both the
57 post-emplacement deformation of an ignimbrite and the pre-emplacement palaeo-
58 topography.

59

60 In this study we use the deformed large-volume ($>1260 \text{ km}^3$; García et al. (2004))
61 Cardones ignimbrite, dated at 21.9 Ma (van Zalinge et al. 2016) to reconstruct the pre-
62 and post-eruptive deformation of the Western Andean Slope in northernmost Chile.
63 The ignimbrite buries underlying palaeo-topography across the Western Andean
64 Slope and is exceptionally well preserved due to the hyperarid climate in the region

65 (e.g. Dunai et al., 2005; Kober et al., 2007; Evenstar et al., 2009). Multiple 1 km-deep
66 drill holes and field outcrops in a 1700 m-deep river valley (the Lluta Quebrada)
67 provide detailed information about the distribution, thickness and deformation of the
68 Cardones as well as its stratigraphic relationship with older and younger lithologies.
69 The timing of local deformation is determined by dating deformed lithologies as well
70 as younger, overlying, undeformed deposits with U-Pb zircon geochronology.
71 Consequently, we quantify and constrain the Cenozoic development of structural
72 relief in the study area, which indicates that growth of the Western Andean Slope in
73 northern Chile had started by ca. 23 Ma. We subsequently place the result in a wider
74 context and discuss the tectonic controls on timing and amount of deformation as well
75 as landscape evolution.

76

77 **GEOLOGICAL BACKGROUND**

78 The Central Andes result from ongoing subduction of the Nazca plate beneath the
79 South American plate since Jurassic time (e.g. Coira et al., 1982; Jordan et al., 1983;
80 Isacks, 1988). In northern Chile (18°- 21°S), the present-day western flank of the
81 Central Andes is typically divided into five morphotectonic units. From west to east,
82 these are: The Coastal Cordillera, the Central Depression, the Precordillera, the
83 Western Cordillera, and the Altiplano (Fig. 1a) (e.g. Muñoz and Charrier, 1996;
84 García and Hérail, 2005; García et al., 2011; Charrier et al., 2013). In this study we
85 focus on the Central Depression, Precordillera and Western Cordillera in
86 northernmost Chile around 18°20'S (Fig 1b and 1c), together termed the Western
87 Andean Slope.

88

89 Within the study area, the Coastal Cordillera is absent and the Central Depression
90 continues across to the Pacific Ocean. Here, the basin is ~45 km wide and reaches a
91 maximum elevation of ~2000 m on its eastern side, where it borders the Precordillera.
92 The Central Depression and Precordillera are separated by the blind west-vergent
93 Ausipar thrust (e.g. Muñoz and Charrier, 1996; García et al., 2004; García and Hérail,
94 2005; Charrier et al., 2013). The Precordillera is ~30 km wide and increases in
95 elevation from ~2000 m to ~4000 m from west to east. This morphotectonic unit is
96 characterized by two N-S trending long-wavelength fold structures known as the
97 Huaylillas Anticline and the Oxaya Anticline, which lie north and south of the Lluta
98 Quebrada, respectively (Fig. 1b). South of the Azapa Quebrada, the Oxaya Anticline
99 merges with the Sucuna Monocline. Two <10 km-wide, elongate basins are located
100 on the eastern limbs of the two anticlines: the Huaylas Basin to the north and the
101 Copaquilla Basin to the south (e.g. García et al., 2004). A narrow fold and thrust belt
102 bounds the Copaquilla Basin and the southern part of the Huaylas Basin to the east,
103 marking the start of the Western Cordillera and the end of the Precordillera (e.g.
104 Muñoz and Charrier, 1996; García et al., 2004; García and Hérail, 2005). East of the
105 Oxaya Anticline, this fold and thrust belt gives rise to the 4500–5000 m-high Belen
106 ridge, which is absent to the east of the Huaylillas Anticline. The active volcanic arc
107 has been located along the Western Cordillera since the Oligocene (e.g. Coira et al.,
108 1982; Mamani et al., 2010), giving rise to peaks up to 6350 m in elevation (e.g.
109 García and Hérail, 2005).

110

111 **Stratigraphy and Cenozoic Deformation History**

112 Lithologies in the study area (Fig. 1c) range in age from Jurassic to Pliocene. The
113 simplified stratigraphy is presented in Figure 2. In the Precordillera, basement rocks

114 consist of Jurassic-Cretaceous sediments intruded by the late Cretaceous-Palaeocene
115 Lluta batholith (e.g. García et al., 2004). The basement rocks crop out in places where
116 the Precordillera is deeply incised by rivers (Fig. 1b). During the Eocene - Oligocene
117 a period of flat-slab subduction with a convergence rate of 60–100 mm/year (Somoza,
118 1998) is thought to have triggered incipient uplift of the Western Andean Slope (e.g.
119 Isacks, 1988; Lamb and Hoke, 1997; Wörner et al., 2000a; Kay and Coira, 2009;
120 Martinod et al., 2010). During this time, basement rocks were exhumed and uplifted
121 in the Precordillera while contemporaneous accommodation space was created in the
122 Central Depression. Fluvial-alluvial sediments (the Azapa Formation) shed from this
123 emerging palaeo-Precordillera were transported westward and deposited in the
124 Central Depression (Fig. 2) (e.g. Wörner et al., 2002; García et al., 2004; García and
125 Hérail, 2005; Wotzlaw et al., 2011).

126

127 In the late Oligocene, the subducting slab steepened and the convergence rate
128 increased to ~150 mm/yr (Somoza, 1998), associated with a major pulse of silicic
129 ignimbrite volcanism in the early Miocene (e.g. Isacks, 1988; Wörner et al., 2000a;
130 Hoke and Lamb, 2007; Kay and Coira, 2009). A series of large-volume ignimbrites,
131 known as the Oxaya Formation, were emplaced on the Western Cordillera,
132 Precordillera and the Central Depression. The caldera complexes associated with
133 these ignimbrites have not been definitively identified, but their sources were likely
134 located to the east of the study area (García et al., 2000). In the Precordillera and the
135 Central Depression, the Oxaya Formation was deposited between 22.7 and 19.7 Ma
136 and consists of five members that are, from oldest to youngest: the Poconchile
137 ignimbrite, the volcaniclastic Member, the Cardones ignimbrite, the Molinos
138 ignimbrite, and the Oxaya ignimbrite (e.g. Wörner et al., 2000a; García et al. 2004;

139 van Zalinge et al. 2016). The Lupica Formation, located in the Western Cordillera is
140 thought to be the eastern, more proximal equivalent of the Oxaya Formation (García
141 et al., 2004). During the mid-late Miocene, ignimbrite volcanism waned and
142 volcanism in the region was characterised by mafic shield and dome volcanoes (e.g.
143 Wörner et al., 2000a).

144

145 In the Central Depression, ignimbrites of the Oxaya Formation are overlain by
146 sediments of the mid-Miocene El Diablo Formation. Two members are recognized
147 within the El Diablo Formation (García et al, 2004 and references herein). The Lower
148 Member consists of conglomerates, sandstones, siltstones and limestones deposited in
149 a low-energy floodplain and lake basin environment. Clasts in the conglomerates are
150 mainly derived from the Oxaya Formation. The Upper Member comprises layers of
151 gravel predominantly sourced from Mid-Miocene andesitic volcanic rocks in the Pre-
152 and Western Cordilleras deposited in a high-energy fluvial environment. The Upper
153 Member is not present north of the Lluta Quebrada (Fig. 1b). The ages of andesitic
154 clasts indicate that the minimum age of the El Diablo Formation is ca. 12 Ma (García
155 et al., 2004).

156

157 After emplacement of the Oxaya Formation, contractional deformation generated a
158 series of N-S trending long-wavelength anticlines in the Precordillera and a narrow
159 fold and thrust belt in the Western Cordillera (e.g. Muñoz and Charrier, 1996; Wörner
160 et al., 2000; Wörner et al., 2002; García and Hérail, 2005). Deformation inhibited
161 westward transportation of sediment shedding from Andes, which were trapped in
162 two sedimentary basins, the Huaylas and Copaquilla, which formed on the eastern
163 limbs of the Oxaya and Huaylillas Anticlines (e.g. Wörner et al., 2002; García and

164 Hérail, 2005). Growth of the Oxaya Anticline is estimated to have occurred between
165 ca. 10 and 12 Ma (Wörner et al., 2000; Wörner et al., 2002; García and Hérail, 2005),
166 but the exact folding time window for the Huaylillas Anticline is not known. The
167 Huaylas and Copaquilla Basin were filled with up to 350 m-thick late Miocene-
168 Pliocene syn- and post-deformation fluvial, alluvial and lacustrine sediments, known
169 as the Huaylas Formation (Figs. 1 and 2) (e.g. Salas et al., 1966; Wörner et al., 2002;
170 García et al., 2004; García and Hérail, 2005). In the Copaquilla Basin, the Huaylas
171 Formation is typically divided into an Upper Member and a Lower Member (García et
172 al., 2004). The Lower member comprises a series of gravels, conglomerates and
173 sandstones in the form of syn-deformation growth-strata related to the formation of
174 the Oxaya Anticline (García and Hérail, 2005). By contrast, the Upper member
175 consists of horizontal gravels and conglomerates, interpreted as post-deformation
176 deposits (García and Hérail, 2005). In the Huaylas Basin, the Huaylas Formation
177 comprises three members: the Lower, Middle, and Upper Member (e.g. Salas et al.,
178 1966; García and Hérail, 2005). The Lower Member is characterised by fluvial
179 conglomerates and gravels derived from the east. The Middle Member is a succession
180 of finely stratified claystones, siltstones, sandstones, diatomite and bentonite that are
181 interbedded with volcanic rocks. The Upper Member is only observed locally and
182 consists of limestones interbedded with siltstones and sandstones. Both the Oxaya and
183 Huaylas Formations are covered by the late Pliocene Lauca ignimbrite dated at 2.7
184 Ma (e.g. Wörner et al., 2000) (Figs 1c and 2).

185

186 **METHODS**

187 To constrain the deformation history of an ignimbrite using a line-balanced technique,
188 the original ignimbrite surface must first be identified. If any erosion of the surface

189 has occurred, its full extent can be reconstructed by extrapolating between mapped
190 exposures. The internal stratigraphy of the ignimbrites can be used to estimate how
191 much of the surface may have been lost by erosion. Once the original surface of the
192 ignimbrite has been identified, a line-balanced technique can be used to constrain
193 post-emplacement deformation and quantify the generation of structural relief growth.

194

195 Prior to performing the line-balanced reconstruction, a suitable initial surface slope
196 needs to be identified. The surface slope of an ignimbrite directly after emplacement
197 can be estimated by measuring the ratio between the vertical height that a pyroclastic
198 flow descends (H) and its horizontal run out distance (L) (Sparks, 1976; Hayashi and
199 Self, 1992). On average, large ignimbrites have a H/L of 0.02, which corresponds to a
200 surface slope of 1.15° (Sparks, 1976). To further investigate suitable values for
201 original surface slopes of ignimbrites we collated data on ten young undeformed
202 extra-caldera ignimbrites (Table 1). Slope values were either directly taken from the
203 literature or were determined by overlying existing ignimbrite distribution maps on
204 Google Earth topographic imagery, enabling H/L to be calculated. The results
205 demonstrate that original surface slopes of young undeformed ignimbrites are
206 typically $<2^\circ$, although some of the older ignimbrites listed in Table 1 have slightly
207 steeper slopes, which might have been affected by post-deposition deformation.

208

209 The results of the line-balanced reconstruction can be used to determine the palaeo-
210 topography covered by the ignimbrite. However, this requires identification of the
211 base of the ignimbrite and measurement of its full thickness. The internal stratigraphy
212 of the ignimbrite can be then used to confirm the reconstructed palaeo-topography.

213

214 The age difference between the deformed ignimbrite and undeformed overlying
215 deposits provides a maximum time constraint for the duration of deformation since
216 ignimbrite emplacement. By combining this duration with the estimated amount of
217 structural relief growth over the time period, local rates of relief growth can be
218 calculated. To date the undeformed volcanic deposits we use U-Pb zircon
219 geochronology. Zircons were extracted from pumice falls, ash falls and pyroclastic
220 surge and flow deposits using conventional mineral separation techniques and
221 individual grains were then handpicked and annealed in a quartz dish in a furnace at
222 900°C for 60 hours. Representative zircons from each sample were mounted in epoxy
223 resin, polished to expose the grain interiors, and imaged using a Centaurus
224 cathodoluminescence (CL) detector on a Hitachi S3500N scanning electron
225 microscope (SEM) at the University of Bristol. U-Pb zircon analyses were performed
226 at the Natural Environment Research Council Isotope Geosciences Laboratory
227 (NIGL) in Keyworth, UK. $^{206}\text{Pb}/^{238}\text{U}$ and $^{207}\text{Pb}/^{235}\text{U}$ ages were obtained with a Nu
228 Instruments “Nu Plasma” high-resolution multicollector, inductively coupled plasma
229 mass spectrometer connected to a New Wave Research 193FX excimer laser ablation
230 system (LA-MC-ICP-MS). Analytical points had a spot size diameter of 35 μm and
231 up to two points were analysed in each grain. The standard- sampling bracketing
232 technique with primary standard 91500 (1063.6 ± 1.4 Ma; Schoene et al. (2006) and
233 secondary standard Mud Tank (732 Ma; Black and Gulson (1978)) was used to
234 normalise $^{206}\text{Pb} - ^{238}\text{U}$ and $^{207}\text{Pb} - ^{235}\text{U}$ ratios. U-Pb data were reduced with in-house
235 spreadsheets at NIGL and plotted with Isoplot version 4.1 (Ludwig, 2003). Full
236 details about the methodology can be found in Table A1. In addition, four zircons
237 were analysed with whole grain high-precision U-Pb zircon isotope dilution-thermal

238 ionisation mass spectrometry (ID-TIMS), also at NIGL. The method is fully described
239 in van Zalinge et al. (2016).

240

241 To determine eruption ages, we use the reproducibility of single $^{206}\text{Pb}/^{238}\text{U}$ dates that
242 define the youngest coherent population. This is evaluated through calculating
243 weighted mean ages with acceptable mean square weighted deviation (MSWD)
244 values according to the method of Wendt and Carl (1991).

245

246 **DATA**

247 The Cardones ignimbrite covers a total area of more than 4200 km² (García et al.,
248 2004) and in the study area (ca. 1000 km²) it entirely buries the underlying palaeo-
249 topography (Fig. 1b, 2 and 3a). Before presenting the results of the line-balanced
250 reconstruction we: (a) describe the internal stratigraphy of the Cardones ignimbrite;
251 (b) describe the present-day configuration of the Cardones ignimbrite, including
252 thickness, deformation and its relationship with underlying and overlying lithologies;
253 and (c) identify undeformed lithologies that can be used to constrain the duration of
254 deformation. The data are based on observations from both the drill cores and
255 outcrops in the Lluta Quebrada.

256

257 **The Cardones Ignimbrite – Internal Stratigraphy**

258 Based on drill core observations, the Cardones ignimbrite comprises two units; their
259 internal structure is described in detail in van Zalinge et al. (2016). The lower unit
260 (unit 1) is the most extensive, thickest and best preserved (Fig. 3a). Based on
261 lithologies and textures of lithic and juvenile clasts, four transitional subunits are
262 recognised in unit 1, which are from base to top: subunit 1; subunit 2; subunit 3 and

263 subunit 4. Subunit 1 is weakly to moderately welded and contains less than 30%
264 crystals, 1% juvenile clasts, and 2% lithic clasts (mainly granite and andesite).
265 Subunit 2 is moderately welded and contains on average 50% crystals, 3% juvenile
266 clasts, and up to 4% lithic clasts (mainly granite and andesite). Subunit 3 is strongly
267 welded and has similar characteristics to subunit 2, but only contains 0.2% lithic
268 clasts. Subunit 4 is weakly welded to unwelded and contains on average 40% crystals,
269 10% juvenile clasts and 5% lithic clasts (mainly dacite and rhyolite). Welding and
270 compaction as a result of pore-space reduction in pumice and matrix of unit 1 resulted
271 in an ignimbrite thickness reduction of ca. 30% (van Zalinge et al, 2016). In particular
272 the strongly welded subunit 3 contributes ca. 60% to the thickness reduction. The
273 unwelded top of subunit 4 is considered to be the original surface of unit 1 and will be
274 used in the line-balanced reconstruction.

275

276 **The Cardones Ignimbrite – Present-Day Configuration**

277 The present-day configuration of the Cardones ignimbrite across the Central
278 Depression, Precordillera and Huaylas Basin, north of the Lluta Quebrada is presented
279 in an orogen-perpendicular cross-section in Figure 3a. The cross-section includes the
280 location of the seven drill cores in the Precordillera as well as the location of the
281 Molinos field section in the Central Depression. The Molinos section is the only
282 easily accessible field location for sampling the Oxaya Formation in the steep
283 northern wall of the Lluta Quebrada (García et al. 2004; van Zalinge et al. 2016).

284

285 ***The Central Depression - West of the Molinos Section***

286 Across the Central Depression, the unwelded top of the Cardones ignimbrite can be
287 clearly recognised in the field, and thus the full thickness of unit 1 is preserved. West

288 of the Molinos section, only the upper sequence of the Oxaya Formation (i.e. the
289 Oxaya ignimbrite, the Molinos ignimbrite, and the upper part of the Cardones
290 ignimbrite) crops out in the Lluta Quebrada (Fig. 3b). The sequence, including the
291 upper surface of the Cardones ignimbrite, dips westward with an average angle of
292 1.3°; no overt deformation can be recognised.

293

294 *The Central Depression - From the Molinos Section to Hole 7*

295 Between the Molinos section and the Ausipar thrust, both the Oxaya Formation and
296 the top of the underlying Azapa Formation crop out in the Lluta Valley. The whole
297 exposed sequence, including the surface of the Cardones ignimbrite, has an average
298 westward dip of ca. 4°. The Ausipar thrust cuts and offsets the top of the Azapa
299 Formation and the Poconchile ignimbrite with an estimated vertical throw of ca. 200
300 m and horizontal shortening of ca. 240 m (Fig. 3c). The thrust has a tip-point just
301 above the Poconchile ignimbrite and just below the Cardones ignimbrite (García et
302 al., 2004; García and Hérail, 2005). Consequently, the Cardones ignimbrite is folded
303 into a ~2 km-wide fault propagation flexure dipping up to ca. 20° to the west. Taking
304 this small fold into account, the average surface slope for the Cardones ignimbrite is
305 5.5° between the Molinos section and hole 7. The Cardones ignimbrite gradually
306 thickens towards the east, with a thickness of ca. 300 m near the Molinos section and
307 470 m in hole 7 (Table 2). The Azapa Formation has a thickness greater than 250 m in
308 the Central Depression (the base of the formation is buried and the full thickness is
309 not observed).

310

311 *Precordillera - From Hole 7 to Hole 9*

312 The seven drill holes (7, 4, 2, 1, 5, 6 and 9) lie in a NE-SW line spanning the
313 Precordillera from the eastern edge of the Central Depression to the western margin of
314 the Huaylas Basin. Here, the Cardones ignimbrite is gently folded by the Huaylillas
315 Anticline (Fig. 3a), the hinge of which (between holes 1 and 5) is characterised by a
316 series of sub-vertical NW-SE-trending (azimuth: 138°) fractures (Fig. 3d). Table 2
317 presents the thicknesses of the different subunits in unit 1 in each hole. Subunit 4 and
318 the top part of subunit 3 have been eroded from holes 1 and 5, which are located in
319 the anticlinal hinge zone. The full thickness of the Cardones ignimbrite is preserved
320 on the eastern and western limbs of the anticline. The upper surface has a slope
321 between 5.5° and 6.1° (with an average of 5.7°) on the western limb and 5.7° on the
322 eastern limb. Furthermore, the basal subunits 1 and 2 are laterally discontinuous, as
323 subunit 1 is only present in drill hole 1 and subunit 2 is very thin in hole 9. In the
324 eastern part of the Precordillera (east of hole 1), the Azapa Formation and oldest
325 members of the Oxaya Formation are missing and thus the Cardones ignimbrite
326 directly overlies the Jurassic-Palaeocene basement. The Azapa Formation overlies the
327 basement with a thickness of less than 50 m in holes 1 and 2 and is absent in hole 4.
328 Note that the Azapa Formation is significantly thicker to the west (260 m in hole 7
329 and >250 m in the Central Depression).

330

331 **Huaylas Basin – Identification of Undeformed Deposits**

332 Lying to the east of the Huaylillas Anticline, the Huaylas Basin is a ~6 km-wide and
333 ~20 km-long N-S-trending depression. The basin is filled with Huaylas Formation
334 sediments, which lie above the Oxaya Formation, and are partly covered by the Lauca
335 ignimbrite (Fig. 4). Hole 9 was drilled on the western edge of the Huaylas Basin
336 (Figs. 1c and 3) and sampled a ~90 m-thick sedimentary sequence overlying a

337 pyroclastic sequence (including the Cardones ignimbrite). A detailed stratigraphic log
338 of the top of hole 9 is presented in Figure 5a. The lower ~50 m of the sedimentary
339 interval is characterised by polymict, poorly sorted, matrix supported conglomerates.
340 The clasts are mainly angular to sub-rounded porphyritic andesites and dacites hosted
341 in a reddish-brown sandy matrix. The clasts are commonly altered and range from a
342 few millimetres to tens of centimetres in size. The poorly sorted, immature nature of
343 the clasts indicates that they are locally sourced and deposited by debris flows. These
344 conglomerates are unconformably overlain by a 40 m-thick interval of well-sorted,
345 horizontal, finely-bedded claystones, siltstones, sandstones, diatomite and organic-
346 rich layers interbedded with minor volcanic ash and pumice horizons, indicating a
347 low-energy lacustrine environment. Similar lacustrine deposits have been observed in
348 the field at the Attane Quebrada to the east of hole 9 (Fig. 4). There was no evidence
349 in drill hole 9 or in the field that these lacustrine deposits are deformed.

350

351 **RESULTS**

352 **Reconstruction of the Ignimbrite Surface**

353 Unit 1 of the Cardones ignimbrite is partly eroded in the hinge zone of the Huaylillas
354 Anticline, but well preserved in both anticlinal limbs. We reconstructed the original
355 thickness of unit 1 by extrapolating the present-day 5.7° surface slope of each limb
356 towards the hinge (Fig. 6a). This allowed us to estimate the original thickness of the
357 Cardones ignimbrite in hole 1 (1190 m), hole 5 (770 m), and the hinge of the
358 Huaylillas Anticline. Subtracting the reconstructed thickness from the observed
359 thickness indicates that as much as 560 m of Cardones ignimbrite has been eroded
360 from the fold hinge zone east of hole 2 (Fig. 6a and Table A2). This means that the
361 overlying Molinos and Oxaya ignimbrites must also have been eroded. Furthermore,

362 we extended the upper surface of unit 1 eastwards to a point 'E', where the Western
363 Cordillera begins and the cross-section line intersects a thrust fault mapped by García
364 et al. (2004). We define this point as the eastern edge of the anticline (Figs 3 and 6).

365

366 **Line-Balanced Reconstruction of the Cardones Ignimbrite**

367 The reconstructed surface of unit 1 in the Cardones ignimbrite is used to implement
368 the line-balanced reconstruction method (Fig. 6). First we consider upper and lower
369 bounds on the initial surface slope of the top of unit 1. Observations indicate that most
370 undeformed young ignimbrites have initial surface slopes between 1° and 2° (Table
371 1). Reconstructions using these bounding slope values, however, produced features
372 inconsistent with the geological observations and enabled us to reduce the uncertainty
373 in our estimate of the initial slope. Surface slopes exceeding 1.76° placed the eastern
374 end of the reconstructed profile above the present-day surface, yet there is no
375 evidence for significant subsidence and eastward tilting of the area (e.g. Isacks, 1988;
376 García and Hérail, 2005; Farías et al., 2005; Jordan et al., 2010). Thus, our results
377 suggest that the original surface slope was $<1.8^\circ$. A slope of $<1.2^\circ$ creates two
378 problems for reconstructions. First, the initial slope would be less than the slope of the
379 Cardones ignimbrite in the Central Depression, which we assume to be
380 untilted/undeformed. Second, the top of the Azapa Formation west of hole 7 would
381 dip to the west, when we know from imbricated clasts that sediments were transported
382 from the northeast (García et al, 2004 and references therein). We thus choose to
383 present reconstructions for 1.5° (Fig, 6b) and assume an uncertainty of 0.3° for
384 inferences that are made from the reconstructions of tilting and uplift.

385

386 We chose the Molinos section (location M) as the western pinpoint for the line-
387 balanced reconstruction because no overt deformation has been observed west of the
388 Molinos section. Since we do not have a well-determined absolute pre-Cardones
389 palaeo-elevation for M, all calculated ‘uplift’ is reported as structural relief growth.
390 Thus all determined palaeo-elevations are relative to M, as we do not know how much
391 the forearc may have uplifted and subsided as an isostatic response to contractional
392 deformation and ignimbrite burial. The results of the reconstructions are presented in
393 Table 3 and Figure 6, and the full-dataset can be found in Table A2.

394

395 *Post-Eruptive Deformation*

396 The structural relief growth related to folding was calculated under the assumption
397 that all folding occurred due to buckling, with the elevation of point E being fixed. All
398 other relief growth measured at point E was assigned to tilting (Fig 6c). Assuming no
399 erosion, a surface slope of $1.5 \pm 0.3^\circ$ gives a maximum relief generation of $2285 \pm$
400 165 m along the anticlinal hinge. Over a distance of ~ 50 km (from the eastern edge of
401 the Central Depression to the easternmost edge of the Precordillera), the amount of
402 shortening is 220 ± 10 m and therefore the total strain between M and E is about $4 \times$
403 10^{-3} . The amount of relief generated by westward tilting depends on the distance from
404 M (Table 3). At the easternmost point E, the maximum relief generation related to
405 tilting is 225 ± 255 m (Fig. 6b). The Cardones ignimbrite has experienced up to ~ 560
406 m of erosion at the hinge of the anticline during and/or after deformation. By
407 subtracting this erosion from 2285 ± 165 m, we calculate a maximum relief growth
408 after deposition of the Cardones ignimbrite of 1725 ± 165 m. Although the Oxaya and
409 Molinos ignimbrites have also been removed by erosion in the hinge zone, they do not

410 contribute to our estimates of structural relief growth because the Cardones ignimbrite
411 is used as the palaeomarker.

412

413 *Pre-Eruptive Palaeotopography*

414 The base of the Cardones ignimbrite in the reconstructed sections in Figure 6b
415 represents the palaeo-topography prior to ignimbrite emplacement. Key features of
416 this palaeo-topography are: (a) a nearly flat surface west of hole 1 with a westward
417 slope of $0.4 \pm 0.3^\circ$; (b) a 450 ± 150 m-deep palaeo-depression at hole 1; and (c) a
418 surface dipping $3.7 \pm 0.3^\circ$ east of hole 1 (Fig. 6b). Our line-balanced reconstructions
419 imply that the eastern part of the Precordillera had a palaeo-elevation 960 ± 225 m
420 higher than the eastern part of the Central Depression prior to emplacement of the
421 Cardones ignimbrite. This reconstructed palaeo-topography is supported by the
422 presence of subunit 1 in palaeo-lows and the absence of thick basal subunits on
423 palaeo-highs (Fig. 6). The thickness variations in the Cardones ignimbrite with the
424 ponding of lower units in topographic lows, the absence of Azapa sediments east of
425 hole 1, and the thickening of the Azapa sediments to the east towards the Central
426 Depression all indicate that by 21.9 Ma, the Precordillera already had a quite rugged
427 topography which was infilled by the Cardones ignimbrite.

428

429 Finally, we note that in our reconstruction the top surface of the Azapa Formation
430 west of hole 4 has an apparent eastward dip of $1.2 \pm 0.3^\circ$, which is inconsistent with
431 sediment transport from the northeast. We attribute this observation to erosion, which
432 has cut down through the Azapa Formation, leaving a surface that does not represent a
433 single time horizon. Evidence for erosion includes the absence of the Azapa
434 Formation in hole 4 and the absence of the overlying Poconchile ignimbrite in both

435 holes 4 and 1 (van Zalinge et al., 2016). Specifically, the Poconchile ignimbrite
436 should be expected in hole 1, where it would have ponded in the palaeo-depression.
437 Its absence suggests significant erosion of the lower Oxaya and Azapa Formations in
438 hole 1.

439

440 **U-Pb Geochronology of the Oxaya and Huaylas Formations**

441 In order to place constraints on the timing of deformation, we selected samples from
442 hole 9 for U-Pb zircon geochronology, including three samples from the pyroclastic
443 sequence (905, 907 and 908) overlying the Cardones ignimbrite and four volcanic
444 intervals (902, 903, 904 and 906) in the flat-lying undeformed lake sediments. Figure
445 7 shows the ID-TIMS and LA-MC-ICP-MS results for all ^{230}Th -corrected $^{206}\text{Pb}/^{238}\text{U}$
446 dates alongside the stratigraphy of hole 9. All ages are reported at the 2σ confidence
447 level. A minor proportion (for each sample $n < 4$) of the ages were >30 Ma and these
448 are not shown in Figure 5b or included in the discussion as we interpret them as
449 resulting from the incorporation of xenocrystic material. The full dataset along with
450 calculations of weighted mean ages for the youngest coherent zircon population in
451 each sample can be found in Tables A3 – A4 and Appendix 5. After excluding ages
452 >30 Ma, the samples still give a range of $^{206}\text{Pb}/^{238}\text{U}$ ages that exceeds the 2σ
453 analytical uncertainty. This range typically varies from 0.5 to a few million years and
454 may result from magmatic processes (e.g. prolonged crystal growth, incorporation of
455 antecrysts), entrainment of zircon during eruption, transport and sedimentation, or
456 post-depositional Pb-loss (Bowring et al., 2006).

457

458 Samples 908 and 907, collected from the pyroclastic sequence above the Cardones
459 ignimbrite, show a decrease in age upwards in the stratigraphy, with weighted mean

460 ages of 22.179 ± 0.092 Ma and 17.95 ± 0.37 Ma, respectively. Sample 905, collected
461 above these two samples, but still within the pyroclastic sequence, gives a weighted
462 mean age of 22.99 ± 0.11 Ma, significantly older than sample 907. We therefore
463 suggest sample 905 derives from a large ignimbrite clast that was difficult to identify
464 in the one-dimensional drill core, rather than an in-situ deposit. Nevertheless, all ages
465 are consistent with previously published data for the Oxaya and Lupica Formations
466 (e.g. García et al. 2004).

467

468 LA-MC-ICP-MS analyses of samples collected from the lacustrine deposits give
469 significantly younger weighted mean ages than those of the Oxaya Formation. From
470 base to top, these are: 5.80 ± 0.11 Ma (906); 5.894 ± 0.053 Ma (904); 5.909 ± 0.075
471 Ma (903); and 5.69 ± 0.15 Ma (902). Four ID-TIMS $^{206}\text{Pb}/^{238}\text{U}$ dates for sample 903
472 range from 5.396 ± 0.160 to 6.296 ± 0.025 Ma (Table A4), but do not give a
473 statistically valid weighted mean age. Combined, these data constrain deposition of
474 the flat-laying lake deposits to ca. 5.9–5.5 Ma, the latest stage of the Miocene.

475

476 Comparison of our results with previous descriptions of the Huaylas Formation in the
477 Huaylas Basin (Fig. 7b and García et al. (2004)), lead us to correlate the lacustrine
478 sequence with the Middle Member of the Huaylas Formation. The poorly sorted
479 immature conglomerates that we have constrained between ~18 and 6 Ma could be
480 correlated to the syn-deformational Lower Member of the Huaylas Formation in the
481 Copaquilla and Huaylas Basins. However, the limitations of one-dimensional drill
482 core observations do not allow us to identify whether these conglomerates are
483 deposited as a growth stratum related to the formation of the Huaylillas Anticline.
484 Alternatively, the volcanic-rich nature of the clasts may imply these deposits were

485 formed from lahars and could be part of the Oxaya/Lupica Formation. Nevertheless,
486 the lack of ignimbrite clasts favours an interpretation that they are equivalent to the
487 conglomerates of the Lower Member of the Huaylas Formation sourced from the east.

488

489 The Oxaya and Molinos ignimbrites are both missing in hole 9 and there is a potential
490 hiatus in deposition of up to 12 Ma. Consequently, we propose at least one, and
491 possibly more, erosional unconformities between the top of the Cardones ignimbrite
492 and the base of the lacustrine deposits (Fig. 5). Figure 7 shows the temporal
493 relationship between the Huaylas Formation in the Huaylas Basin and the Copaquilla
494 Basin. The onset of gravel sedimentation in the Copaquilla Basin is constrained to
495 ~12 Ma, whereas the onset of sedimentation in the Huaylas Formation is unclear. Our
496 data suggest that infill of the Huaylas Basin could have commenced up to 6 million
497 years earlier, after ~18 Ma. The 10.7 Ma Caragua Tignamar ignimbrite marks the end
498 of the syn-tectonic growth strata in the Copaquilla Basin (Wörner et al., 2000; García
499 and Hérail, 2005), after which minor sedimentation occurred. Data from the Huaylas
500 Basin suggest a change to lacustrine sedimentation conditions around 6 Ma, but such
501 a change is not observed in the Copaquilla Basin. However, the onset of lacustrine
502 sedimentation in the late Miocene is consistent with dating of ashes intercalated with
503 lacustrine Lauca Formation sediments in the Lauca Basin, east of the Belen Ridge
504 (Fig. 1b) (Kött et al, 1995; Gaupp et al. 1999).

505

506 **DISCUSSION**

507 The large volume Oxaya Formation ignimbrites, including the 21.9 Ma Cardones
508 ignimbrite, inundated and buried large parts of northernmost Chile (18-18.5°S) in the
509 early Miocene. Despite significant post-emplacement deformation, some of these

510 ignimbrites are exceptionally well preserved and enable the history of structural relief
511 and topography on the Western Andean Slope to be elucidated. By combining a line-
512 balanced reconstruction of the surface of the Cardones ignimbrite with detailed
513 stratigraphic analysis and high-precision U-Pb zircon geochronology, we show that
514 significant relief generation and fluvial incision on the Western Andean Slope
515 commenced before ca. 22.7 Ma and that the main deformation ceased before 6 Ma
516 (Fig. 8).

517

518 **Pre-21.9 Ma Deformation and Structural Relief Growth**

519 The reconstructed pre-eruptive palaeo-topography reveals the existence of a palaeo-
520 slope on the western flank of the Central Andes prior to 21.9 Ma. This slope dipped
521 $3.7 \pm 0.3^\circ$ westward and, in the eastern Precordillera, reached an elevation up to $960 \pm$
522 225 m higher than the eastern margin of the Central Depression. In the eastern
523 Precordillera, this palaeo-surface was characterized by exhumed basement lithologies
524 (Figs 3 and 6). In the western Precordillera, the basement dipped westward with an
525 apparent slope of $0.4 \pm 0.3^\circ$ and was unconformably overlain by coarse Azapa
526 sediments that thickened to the west. We suggest that this pre-21.9 Ma palaeo-
527 topography reflects contemporaneous structural relief growth and erosion in the
528 Precordillera and the creation of accommodation space and sedimentation in the
529 Central Depression, much as is seen in the region today (Fig. 8a).

530

531 Our work concurs with previous interpretations that deformation prior to the early
532 Miocene ignimbrite flare up included an episode of thrusting along the Ausipar thrust,
533 which uplifted the Precordillera and created accommodation space in the Central
534 Depression (e.g. Muñoz and Charrier, 1997; Wörner et al. 2002; García and Hérail et

535 al. 2005; Charrier et al., 2013). This uplift resulted in erosion of both the Pre-and
536 Western Cordillera and deposition of a thick sequence of coarse clastic sediments (the
537 Azapa Formation) in the Central Depression (Figs. 8a). Wörner et al. (2002)
538 suggested that these sediments were sourced from the western flank of a proto-
539 Altiplano before 22.7 Ma (the age of the Poconchile ignimbrite, which directly
540 overlies the Azapa Formation, Figure 2), and our observations are consistent with this
541 interpretation. Consequently, we suggest that our reconstructed palaeo-slope (Fig. 8a)
542 reflects initial growth of a proto- Western Andean Slope in the study area. In order to
543 put better time constraints on the development of this slope, we refer to a provenance
544 study of the Azapa Formation performed by Wotzlaw et al. (2011). This study showed
545 that detrital zircons from the Azapa Formation were mostly Paleocene-Cretaceous
546 (60-80 Ma) in age, but included some Eocene (35-50 Ma) material. Consequently,
547 deposition of the Azapa Formation, and therefore initial growth of a proto-Western
548 Andean Slope, can be constrained to between ~35 and 22.7 Ma (Fig. 8a).

549

550 The line-balanced reconstruction (Fig. 6b) suggests the presence of a 450 ± 150 m-
551 deep palaeo-depression near hole 1, which was subsequently infilled by the Cardones
552 ignimbrite. We interpret this depression to be a river valley and propose, following
553 the principles described in Montgomery and Brandon (2002), that river incision in the
554 Precordillera at this time occurred as a response to exhumation and uplift of the
555 palaeo-Western Andean Slope (Fig 6b and 8a).

556

557 **Post-21.9 Ma Deformation and Structural Relief Growth**

558 Geological structures observed in the field, such as the Ausipar thrust and the
559 Huaylillas Anticline, together with our line-balanced reconstruction indicate that the

560 study area experienced significant structural relief growth after eruption of the Oxaya
561 Formation ignimbrites. Whether this relief generation was a continuation of the
562 deformation that occurred prior to 21.9 Ma, or was a separate deformation event, is
563 unclear from our results. Nevertheless, field observations and satellite imagery of the
564 Ausipar thrust (Fig. 3c) suggest that the latest phase of movement on the structure
565 occurred after emplacement of the 19.7 Ma Oxaya ignimbrite. Furthermore, the entire
566 Oxaya Formation is clearly folded. We therefore conclude that after emplacement of
567 the Oxaya Formation, the study area was faulted, folded and tilted, resulting in the
568 generation of up to 1725 ± 165 m of structural relief and E-W shortening of 220 ± 10
569 m in the present-day Precordillera, north of the Lluta Quebrada. This result is
570 consistent with the 1700 m-deep incision observed in the Lluta Quebrada (García et
571 al., 2011) with growth of the fold crest compensated by incision of the river. We note
572 that this estimate assumes that the upper surface of the Cardones ignimbrite was
573 planar and does not account for changes in relief related to welding compaction. With
574 compaction estimated at a 30% reduction in thickness (van Zalinge et al., 2016), the
575 relief could have been a few tens of metres lower in the area of greatest original
576 thickness. This effect would slightly increase the estimate of structural relief growth
577 during contractional deformation.

578

579 If erosion of the hinge of the Huaylillas Anticline had not occurred, structural relief
580 generation could have been as much as 2285 ± 165 m. Using this result, we calculate
581 the fold amplitude by subtracting the tilt-related uplift. This gives a fold amplitude of
582 2140 m, which is independent of the assumed initial surface slope (Table 3). At least
583 90% and as much as 100% of the structural relief generation at the hinge of the
584 anticline can be assigned to folding. The remaining 0–10% of relief generation is

585 attributed to westward tilting of the Precordillera. We calculate that the Precordillera
586 experienced $0.3^\circ \pm 0.3^\circ$ of westward tilting, which, over a distance of ca. 50 km,
587 results in an uplift of 225 ± 255 m on the eastern edge of the Precordillera (Table 3).
588 In the following section, the timing and folding intensity of the Huaylillas Anticline
589 with respect to the Oxaya Anticline is discussed in more detail.

590

591 **Landscape evolution related to ignimbrite emplacement and anticline formation**

592 We have already presented evidence that, prior to ignimbrite emplacement at 21.9
593 Ma, the Precordillera dipped $3.7 \pm 0.3^\circ$ to the west and was cut by a 450 ± 150 m-
594 deep palaeo-valley. In this section we will further argue that a valley in the location of
595 the present-day Lluta Quebrada started to incise directly after emplacement of the
596 early Miocene ignimbrites. This interpretation differs from those of Wörner et al.
597 (2002) and García and Hérail (2005) that incision of the Lluta Quebrada commenced
598 after ca. 12 Ma in response to anticline formation. Here we discuss further how the
599 landscape responded to inundation by the ignimbrites and formation of the anticlines.

600

601 First, any pre-eruptive river system will be buried by the ignimbrite. Once surface
602 waters are able to establish a new channel network, this river system will be out of
603 equilibrium because the ignimbrite has changed the surface profile. Equilibrium river
604 profiles are typically concave (up) where channel slope decreases with distance
605 downstream. By contrast, ignimbrites are generally deposited with approximately
606 constant slopes (Table 1), and thus the initial post-emplacement river profiles are too
607 shallow in upstream regions and too steep in downstream regions. The Oxaya
608 Formation ignimbrites are in general thickest in the Precordillera and thin towards the
609 Pacific. Consequently, the source of a river in the east would have increased in

610 elevation relative to its base level in the west. This change would have perturbed the
611 fluvial drainage system, causing it to incise predominantly in the Precordillera in
612 order to re-establish an equilibrium profile. Evidence from very young ignimbrites
613 (e.g. Wilson, 1991) shows that post-eruption incision tends to occur most rapidly into
614 the unwelded top of the ignimbrite (within a few years or decades), but then slows
615 down when it reaches the strongly welded ignimbrite beneath.

616

617 The second major effect of ignimbrites on landscape evolution relates to welding
618 compaction. The pre-21.9 Ma palaeo-valley (Fig. 6b) is located in a similar location
619 to the present-day Lluta Quebrada. When large-volume ignimbrites are first emplaced
620 they infill topography with a level upper surface. However, during welding the
621 compaction is greatest where the ignimbrite is thickest (e.g. infilled palaeo-valleys),
622 creating an embryonic topography that controls the location of future river incision
623 (Fig. 8b). Van Zalinge et al. (2016) calculated that compaction of the Cardones
624 ignimbrite reduced its thickness by about ~30%. For example, a ~1000 m thick
625 deposit in a palaeo-valley would lose ~300 m of thickness as a result of compaction,
626 whereas a ~500 m thick deposit on a palaeo-high would lose 150 m of its initial
627 thickness (Fig. 8b). Thus, a 150 m deep embryonic depression is formed over the pre-
628 eruption valley enabling the pre-eruption drainage to be re-established. Infilling of
629 pre-eruption valleys by ignimbrites and re-exhumation of these ignimbrites to form
630 valleys in approximately the same place is commonly observed (e.g. Sparks, 1975;
631 Myers, 1976). These arguments suggest that formation of the Lluta Quebrada began
632 prior to folding.

633

634 We now consider the evolution of the landscape related to formation of the anticlines
635 and explore the effect of the landscape on folding. Previous studies attributed growth
636 of the Oxaya Anticline to a ~2 million year time window in the middle Miocene using
637 age constraints from the Huaylas and El Diablo Formations (Wörner et al., 2000a;
638 Wörner et al., 2002; García and Hérail, 2005). The lower part of the Huaylas
639 Formation in the Copaquilla Basin is defined by growth strata related to formation of
640 the Oxaya Anticline (Fig. 7c). A folded lava flow that overlies the Oxaya ignimbrite,
641 but underlies the growth strata of the Huaylas Formation, was dated at 11.7 ± 0.7 Ma
642 (García and Hérail, 2005), suggesting that folding must have started after deposition
643 of this lava. The end of folding of the anticline is constrained by the flat-lying $10.7 \pm$
644 0.3 Ma Tignamar ignimbrite (Wörner et al. 2002; García and Hérail, 2005) that
645 overlies growth strata in the Huaylas Formation (Fig 7). The onset of folding
646 determined from the Copaquilla Basin is compatible with the ca. 12 Ma minimum age
647 of the Upper Member of the El Diablo Formation west of the Oxaya Anticline (García
648 et al., 2005). This minimum age is consistent with cosmogenic exposure ages of the
649 depositional surface of the El Diablo Formation, which cluster around 12 Ma (data
650 initially presented in Evenstar et al., 2009 and recalculated in Evenstar et al., 2015).
651 Since the Upper Member of the El Diablo Formation is sourced to the east of the
652 Oxaya Anticline (e.g. Wörner et al., 2000), this led García and Hérail (2005) to
653 suggest that the topographic barrier created by the anticlinal hinge cannot have
654 existed prior to 12 Ma.

655

656 However, there are a number of reasons why folding could have commenced prior to
657 ca. 12 Ma. Firstly, our reconstruction demonstrates that immediately after eruption,
658 the ignimbrites had a west-dipping, $1.5 \pm 0.3^\circ$ surface that was subsequently deformed

659 by folding. The topographic barrier defined by the hinge zone of the anticline could
660 not have formed immediately as it would have taken some time for the eastern limb of
661 the fold to rotate from a westward to an eastward dip and form the Copaquilla and
662 Huaylas Basins. We can thus conclude that folding could have started prior to 12 Ma.
663 Furthermore, during this initial deformation phase, fluvial incision into the anticline
664 could have kept pace with its structural growth, forming a series of channels linking
665 the Precordillera/Western Cordillera to the Central Depression. Previous studies (e.g.
666 Wörner et al. 2000, 2002; García and Hérail, 2005) suggested that the Azapa and
667 Lluta Quebradas cut through the upper surface of the El Diablo Formation and thus
668 that river incision commenced after ca. 12 Ma. However, this observation only
669 demonstrates that incision continued after deposition of the El Diablo Formation in
670 the Central Depression, and does not preclude earlier incision into the Precordillera.
671 We suggest it is likely that during initial formation of the anticlines, river incision was
672 able to keep pace with uplift, transporting El Diablo Formation sediments westward to
673 the Central Depression. Deposition of these sediments was confined to the western
674 margin of the anticlines where accommodation space was available (Fig. 9). After 12
675 Ma continued growth of the anticlines created a topographic barrier that confined
676 sediments to the basins on the eastern margin of the anticlines.

677

678 Landscape evolution of the region is inferred to be markedly different north and south
679 of the Lluta Quebrada. In particular, the anticlinal fold hinges of the Oxaya and
680 Huaylillas Anticlines appear to be dextrally displaced by >10 km across the Lluta
681 Quebrada (Fig. 9). Furthermore, the appearance of the El Diablo Formation north and
682 south of the Lluta Quebrada is markedly different. We suggest that the intensity and
683 possibly the timing of deformation of the Oxaya and Huaylillas Anticlines are

684 different. Our calculated maximum values for fold amplitude (2140 m) and horizontal
685 E-W shortening (~210 m) for the Huaylillas Anticline are almost three times as large
686 as those calculated for the Oxaya Anticline (fold amplitude: 665–840 m; horizontal
687 shortening 60–80 m) by García and Hérail (2005). These authors used the present-day
688 erosional surface as a palaeo-surface in their reconstructions and did not consider
689 erosion at the hinge of the anticline. Their calculated fold amplitude is therefore likely
690 underestimated. Stratigraphy of the Oxaya ignimbrites shows that the non-welded
691 upper part of the Oxaya ignimbrite has been eroded from the hinge of the Oxaya
692 Anticline. However, even if we account for erosion (maximum of a few hundred
693 metres), the fold amplitude of the Oxaya Anticline remains much less than the
694 Huaylillas Anticline. Consequently, we conclude that the amplitude of folding
695 decreases from the Huaylillas in the north to the Oxaya Anticline and Sucuna
696 Monocline (Fig. 1b) in the south.

697

698 A marked change across the Lluta valley is indicated by differences in the
699 characteristics of surfaces in the region to the west of the anticlines (Fig. 9). The
700 Upper Member of the El Diablo Formation with its characteristic dark surface is
701 absent to the west of the Huaylillas Anticline. Here the surface is pale, and thin
702 deposits (max. a few tens of metres) are mostly reworked products of the Oxaya
703 Formation. One interpretation is that these deposits represent the Lower Member of
704 the El Diablo Formation. In this case the depositional age of this Lower Member is
705 constrained by the Oxaya ignimbrite (19.7 Ma) and the minimum age of the Upper
706 Member of the El Diablo Formation (ca. 12 Ma). However, reworking of the
707 ignimbrite could have continued to more recent times and thus the ages of this surface
708 and its deposits are not well constrained. We identify two explanations for the

709 absence of the Upper Member of the El Diablo Formation west of the Huaylillas
710 Anticline. One explanation is that folding of the Huaylillas Anticline initiated earlier
711 than the Oxaya Anticline, trapping Upper Member El Diablo sediments in the
712 Huaylas Basin to the east. A second explanation is that the source rocks for to the east
713 are different north and south of the Lluta Quebrada. However, we note that mid-
714 Miocene andesitic source rocks of the Upper Member of El Diablo Formation are
715 present throughout (purple outcrops in Fig. 1b). Finally, the upper El Diablo
716 sediments could have been transported directly to the Pacific through the gap in the
717 Coastal Cordillera. If this is the case, it raises the question why the Lower Member of
718 the El Diablo Formation wasn't also transported into the Pacific. One possibility is the
719 entire El Diablo Formation is missing north of the Lluta Quebrada and all sediments
720 here are later reworked Oxaya Formation. Based on our ca. 6 Ma age for the
721 undeformed, flat-lying lacustrine deposits in the Huaylas Basin we conclude that the
722 formation of the Huaylillas Anticline must have ceased by ca. 6 Ma.

723

724 Finally, we address the offset in the hinge lines of the Huaylillas and Oxaya
725 Anticlines. An east-west-trending fault along the Lluta Quebrada can be firmly ruled
726 out by the absence of any lateral offset of the Ausipar thrust, which is thought to have
727 been active since at least the Eocene (e.g. Muñoz and Charrier, 1996). Instead, we
728 suggest that the Lluta Quebrada already existed before folding initiated and was
729 further incised during fold development. The orientation of the Western Cordillera
730 fold and thrust belt (Fig. 9) to the east of the anticlines gradually changes from NNE-
731 SSW to almost N-S between the Azapa and Lluta Quebradas. While this change could
732 account for some curvature of the Oxaya Anticline hinge zone, it cannot explain the
733 abrupt displacement of the two hinge zones across the Lluta Quebrada. Instead, we

734 propose that, prior to folding, the deep palaeo-valley that had already incised the
735 Oxaya Formation caused the units on either side to act as mechanically independent
736 layers that responded to buckling in different ways. Thus, this is a case of the
737 landscape influencing fold development.

738

739 From our discussion, we conclude that incision of a proto-Lluta River commenced
740 directly after emplacement of the Oxaya Formation ignimbrites. We suggest that
741 formation of both anticlines likely commenced before 12 Ma and the Huaylillas
742 Anticline experienced significantly more structural relief growth compared to the
743 Oxaya Anticline. Based on our ca. 6 Ma age for the undeformed, flat-lying lacustrine
744 deposits in the Huaylas Basin to the east of the Huaylillas Anticline, we conclude that
745 the main phase of folding of the Huaylillas Anticline had ceased by the end of the
746 Miocene (Fig. 8c).

747

748 **Regional implications**

749 Compressional foreland fold geometries like the Huaylillas and Oxaya Anticlines are
750 typically associated with activation of basement faults (e.g. Narr and Suppe, 1994),
751 such as the Ausipar thrust (García and Hérail, 2001). Our results show that between
752 90% and 100% of the structural relief growth in the Precordillera can be attributed to
753 basement-involved fault-propagation folding in response to crustal shortening.
754 Similarly, to the south (~19°–20°S), structural relief growth of the Precordillera is
755 also characterized by west-vergent thrusts that propagate into monoclines and flexures
756 (e.g. Victor et al., 2004; Pinto et al., 2004; Farías et al., 2005). These flexures are
757 thought to have accommodated ~2000 m of relative surface uplift between 19°20'S
758 and 19°50'S (Farías et al., 2005) and ~2600 m of surface uplift around 20°S (Victor et

759 al., 2004). These results are in good agreement with our estimate of up to 2140 m
760 (assuming no erosion) of structural relief growth at the hinge of the Huaylillas
761 Anticline (Table 2).

762

763 The growth of flexures and monoclines around 19°S–20°S was associated with syn-
764 deformation sedimentation. Analyses of growth strata indicate that activity on the
765 faults started as early as 26–30 Ma and lasted until at least 8–7 Ma (Victor et al, 2004;
766 Farías et al., 2005). The onset of deformation in the Oligocene is in good agreement
767 with our reconstructed palaeotopography in northernmost Chile, which indicates that
768 development of the Western Andean Slope commenced before 23 Ma.

769

770 Our estimate of tilting-related uplift between the eastern edge of the Central
771 Depression and the easternmost edge of the Precordillera is 225 ± 255 m (Table 3 and
772 Fig. 6b), which includes the possibility of no tilting. Farías et al. (2005) estimated
773 that, after 10 Ma, the forearc was tilted westward, resulting in additional surface uplift
774 of 500–1400 m over a distance of ca. 60 km from the eastern edge of the Central
775 Depression across the Precordillera into the Western Cordillera. Adjusting their
776 estimate to a distance of ca. 50 km gives a range of 400–1200 m, which is still
777 significantly higher than our estimate. We suggest that Farías et al. (2005)
778 overestimated the amount of uplift related to tilting because they used a palaeo-
779 elevation of 1000 ± 200 m (Charrier et al. 1994) for the Western Cordillera in the late
780 Oligocene-early Miocene. However, our data indicates that the palaeo-elevation of the
781 eastern edge of the Precordillera was possibly up to ca. 1800 m (Table 3).
782 Consequently, we suggest that tilting played a very minor role, and possibly no role,
783 in Neogene uplift of the Western Andean Slope.

784

785 Our results indicate that development of the Western Andean Slope in northernmost
786 Chile has spanned at least parts of both the Oligocene and Miocene. This is
787 compatible with other studies in northern Chile (18–21°S), which have documented
788 uplift and structural relief growth of the Western Andean Slope from the early
789 Oligocene (~30 Ma) to the late Miocene (~6 Ma), after which structural relief
790 generation diminished (Pinto et al., 2004; Victor et al., 2004; Farías et al., 2005;
791 García and Hérail, 2005; Jordan et al., 2010). Our findings are also consistent with
792 geochemical variations in volcanic rocks around the Central Andean orocline (13–
793 18°S) that indicate continuous crustal thickening over the past 30 million years
794 (Mamani et al., 2010). In addition, Decou et al. (2013) suggested that sedimentation
795 in the Peruvian forearc (15–18°S) occurred between ~50 and ~4 Ma, implying that
796 uplift of the Western Andean Slope may have started as early as the Late Eocene. In
797 general, our study is consistent with slow and steady models for Central Andean uplift
798 over the past ca. 40 million years (e.g. Cooper et al., 2016; Evenstar et al., 2015;
799 Barnes and Ehlers, 2009; Lamb and Davis, 2003).

800

801 Overall, studies have shown that Eocene-Oligocene deformation and uplift of the
802 Western Andean Slope and the Altiplano were mainly accommodated by crustal
803 shortening, while addition of significant volumes of magma to the crust and perhaps
804 detachment of the lower crust may also have played important roles during the
805 Miocene (e.g. Isacks, 1988; Lamb and Hoke, 1997; Victor et al., 2004; McQuarrie et
806 al., 2005; Hoke and Lamb, 2007). Evidence for large volumes of magma in the crust
807 includes the Miocene ignimbrite volcanism studied here as well as mafic backarc
808 volcanism in the Altiplano, both of which are contemporaneous with development of

809 the Western Andean Slope (e.g. De Silva, 1989; Wörner et al., 2000a; Victor et al.,
810 2004; Hoke and Lamb, 2007; Kay and Coira, 2009; Freymuth et al., 2015). One
811 possibility is that the associated crustal magmatism heated and weakened the crust
812 along the volcanic front, making it a focal point for deformation (e.g. Isacks, 1988;
813 Allmendinger et al., 1997; Lamb and Hoke, 1997; Hoke and Lamb, 2007; Kay and
814 Coira, 2009). Crustal heating by igneous intrusions below the Altiplano may have
815 resulted in a ductile zone that pinched out beneath the forearc and could have
816 contributed to uplift of the Altiplano.

817

818 Several studies (e.g. Isacks, 1988; Lamb et al., 1996) present tectonic models that
819 invoke tilting of the forearc. However, we find that regional tilting of the forearc
820 played only a minor or no role in our study area. Thus, inferences of little or no
821 surface tilting across the Precordillera suggest that each of the morphotectonic units
822 acted as fault bounded blocks with uplift resulting from shortening combined with
823 largely vertical movements along thrust faults that bound the units. In our study area,
824 the Precordillera is bound by the Ausipar thrust to the west with a vertical
825 displacement of 200 m and thrust faults of the Western Cordillera to the east.

826

827 **CONCLUSIONS**

828 In this study we used the surface of the deformed early Miocene Cardones ignimbrite
829 in northern Chile to reconstruct the pre-eruption palaeo-topography and quantify post-
830 eruption relief growth on the Western Andean Slope. We demonstrate that outflow
831 sheets of large-volume ignimbrites are able to entirely infill and bury the topography
832 of an area, forming planar surfaces with slopes of less than 2°. If well preserved, such

833 ignimbrites are excellent spatial and temporal markers to record post-emplacment
834 deformation.

835

836 Our results suggest that development of the Western Andean Slope in northernmost
837 Chile ($\sim 18^{\circ}20'$) began as early as Oligocene time, most likely in response to crustal
838 shortening and magmatic addition. By ca. 23 Ma, the palaeo-Western Andean Slope
839 was up to 960 ± 225 m higher than in the Central Depression, dipped up to $3.7 \pm 0.3^{\circ}$
840 westward, and was deeply incised by rivers. This dissected landscape was
841 subsequently infilled and submerged by a series of large-volume ignimbrites in the
842 early Miocene. During deposition, the thickest sequences of ignimbrite accumulated
843 in the deep river valleys. Subsequently, these thick ignimbrites became the most
844 strongly welded and compacted, creating a topographic depression that focused
845 subsequent river incision into similar locations as the pre-ignimbrite palaeo-valleys.
846 After deposition of the Oxaya Formation, the Western Andean Slope experienced a
847 maximum 1725 ± 165 m of structural relief growth largely, if not entirely, related to
848 folding in response to contractional deformation. Based on new U-Pb age constraints
849 on volcanic horizons in flat-lying lake sediments, we determined that this folding
850 must have ceased by ca. 6 Ma. Andean uplift as a result of regional tilting, however,
851 is significantly less than previously estimated (e.g. Lamb et al. 1996; Farias et al.
852 2005) and could have been zero.

853

854 **ACKNOWLEDGMENTS**

855 This project was funded by BHP Billiton. We would like to thank all people at BHPB,
856 especially Christopher Ford, who provided support in the field and core shed. Funding
857 for U-Pb zircon analyses was provided by Natural Environment Research Council

858 NIGFC grant IP-1466-1114 to FJC. Analytical work would not have been possible
859 without technical support from Nick Roberts, Vanessa Pashley, Simon Tapster, and
860 Nicola Atkinson. The manuscript has benefitted from constructive reviews by G.
861 Wörner, S. Kay, C. Garziona and two unknown reviewers.

862

863 **REFERENCES**

864 Aldiss, D., and Ghazali, S., 1984, The regional geology and evolution of the Toba
865 volcano-tectonic depression, Indonesia: *Journal of the Geological Society*, v. 141, no.
866 3, p. 487-500.

867

868 Allmendinger, R. W., Jordan, T. E., Kay, S. M., and Isacks, B. L., 1997, The
869 evolution of the Altiplano-Puna plateau of the Central Andes: *Annual review of earth
870 and planetary sciences*, v. 25, no. 1, p. 139-174.

871

872 Barnes, J., and Ehlers, T., 2009, End member models for Andean Plateau uplift:
873 *Earth-Science Reviews*, v. 97, no. 1, p. 105-132.

874

875 Best, M. G., Barr, D. L., Christiansen, E. H., Gromme, S., Deino, A. L., and Tingey,
876 D. G., 2009, The Great Basin Altiplano during the middle Cenozoic ignimbrite
877 flareup: Insights from volcanic rocks: *International Geology Review*, v. 51, no. 7-8, p.
878 589-633.

879

880 Black, L., and Gulson, B., 1978, The age of the mud tank carbonatite, strangways
881 range, northern territory: *BMR Journal of Australian Geology and Geophysics*, v. 3,
882 no. 3, p. 227-232.

883

884 Bond, A., and Sparks, R., 1976, The Minoan eruption of Santorini, Greece: *Journal of*
885 *the Geological Society*, v. 132, no. 1, p. 1-16.

886

887 Bowring, S., Schoene, B., Crowley, J., Ramezani, J., and Condon, D., 2006, High-
888 precision U-Pb zircon geochronology and the stratigraphic record: *Progress and*
889 *promise: Paleontological Society Papers*, v. 12, p. 25.

890

891 Carrasco-Núñez, G., and Branney, M. J., 2005, Progressive assembly of a massive
892 layer of ignimbrite with a normal-to-reverse compositional zoning: the Zaragoza
893 ignimbrite of central Mexico: *Bulletin of Volcanology*, v. 68, no. 1, p. 3-20.

894

895 Cas, R. A., Wright, H. M., Folkes, C. B., Lesti, C., Porreca, M., Giordano, G., and
896 Viramonte, J. G., 2011, The flow dynamics of an extremely large volume pyroclastic
897 flow, the 2.08-Ma Cerro Galán Ignimbrite, NW Argentina, and comparison with other
898 flow types: *Bulletin of Volcanology*, v. 73, no. 10, p. 1583-1609.

899

900 Charrier, R., Muñoz, N., and Palma-Heldt, S., Edad y contenido paleoflorístico de la
901 Formación Chucal y condiciones paleoclimáticas para el Oligoceno Tardío-Mioceno
902 Inferior en el Altiplano de Arica, Chile, in *Proceedings Congreso Geológico*
903 *Chileno 1994*, Volume 1.

904

905 Charrier, R., Hérial, G., Pinto, L., García, M., Riquelme, R., Farías, M., and Muñoz,
906 N., 2013, Cenozoic tectonic evolution in the Central Andes in northern Chile and west

907 central Bolivia: implications for paleogeographic, magmatic and mountain building
908 evolution: *International Journal of Earth Sciences*, v. 102, no. 1, p. 235-264.

909

910 Coira, B., Davidson, J., Mpodozis, C., and Ramos, V., 1982, Tectonic and magmatic
911 evolution of the Andes of northern Argentina and Chile: *Earth-Science Reviews*, v.
912 18, no. 3, p. 303-332.

913

914 Cooper, F.J., Adams, B.A., Blundy, J.D., Farley, K.A., McKeon, R.E., A.A.
915 Ruggiero, 2016, Aridity-induced Miocene canyon incision in the Central Andes,
916 *Geology*, v. 44, doi: 10.1130/G38254.1.

917

918 De Silva, S., 1989, Altiplano-Puna volcanic complex of the central Andes: *Geology*,
919 v. 17, no. 12, p. 1102-1106.

920

921 Decou, A., Von Eynatten, H., Dunkl, I., Frei, D., and Wörner, G., 2013, Late Eocene
922 to Early Miocene Andean uplift inferred from detrital zircon fission track and U–Pb
923 dating of Cenozoic forearc sediments (15–18° S): *Journal of South American Earth
924 Sciences*, v. 45, p. 6-23.

925

926 Dunai, T. J., López, G. A. G., and Juez-Larré, J., 2005, Oligocene–Miocene age of
927 aridity in the Atacama Desert revealed by exposure dating of erosion-sensitive
928 landforms: *Geology*, v. 33, no. 4, p. 321-324.

929

930 Evenstar, L. A., Hartley, A. J., Stuart, F. M., Mather, A. E., Rice, C. M., and Chong,
931 G., 2009, Multiphase development of the Atacama Planation Surface recorded by

932 cosmogenic ^3He exposure ages: Implications for uplift and Cenozoic climate change
933 in western South America: *Geology*, v. 37, no. 1, p. 27-30.

934

935 Evenstar, L. A., Stuart, F. M., Hartley, A. J., and Tattitch, B., 2015, Slow Cenozoic
936 uplift of the western Andean Cordillera indicated by cosmogenic ^3He in alluvial
937 boulders from the Pacific Planation Surface: *Geophysical Research Letters*, v. 42, no.
938 20, p. 8448-8455.

939

940 Farías, M., Charrier, R., Comte, D., Martinod, J., and Hérail, G., 2005, Late Cenozoic
941 deformation and uplift of the western flank of the Altiplano: Evidence from the
942 depositional, tectonic, and geomorphologic evolution and shallow seismic activity
943 (northern Chile at $19^{\circ}30'$ S): *Tectonics*, v. 24, no. 4.

944

945 Freymuth, H., Brandmeier, M., and Wörner, G., 2015, The origin and crust/mantle
946 mass balance of Central Andean ignimbrite magmatism constrained by oxygen and
947 strontium isotopes and erupted volumes: *Contributions to Mineralogy and Petrology*,
948 v. 169, no. 6, p. 1-24.

949

950 García, M., Gardeweg, M., Hérail, G. & Pérez de Arce, C. 2000. La Ignimbrita Oxaya
951 y la Caldera Lauca: un evento explosivo de gran volumen del Mioceno Inferior en la
952 región de Arica (Andes Centrales $18-19^{\circ}$ S). In: IX Congreso Geológico Chileno, 2,
953 Puerto Varas, 286–290.

954

955 García, M., and Hérail, G., 2005, Fault-related folding, drainage network evolution
956 and valley incision during the Neogene in the Andean Precordillera of Northern
957 Chile: *Geomorphology*, v. 65, no. 3, p. 279-300.

958

959 García, M., Gardeweg, M., Clavero, J., and Hérail, G., 2004, Arica map: Tarapacá
960 Region, scale 1: 250,000: *Serv. Nac. Geol. Min.*, v. 84, p. 150.

961

962 García, M., and Hérail, G., 2001, Comment on 'Geochronology (Ar-Ar, K-Ar and He-
963 exposure ages) of Cenozoic magmatic rocks from northern Chile (18-22° S):
964 implications for magmatism and tectonic evolution of the central Andes' of Wörner et
965 al.(2000): *Revista geológica de Chile*, v. 28, no. 1, p. 127-130.

966

967 García, M., Riquelme, R., Farías, M., Hérail, G., and Charrier, R., 2011, Late
968 Miocene–Holocene canyon incision in the western Altiplano, northern Chile: tectonic
969 or climatic forcing?: *Journal of the Geological Society*, v. 168, no. 4, p. 1047-1060.

970

971 Gaupp, R., Kött, A., and Wörner, G., 1999, Palaeoclimatic implications of Mio–
972 Pliocene sedimentation in the high-altitude intra-arc Lauca Basin of northern Chile:
973 *Palaeogeography, Palaeoclimatology, Palaeoecology*, v. 151, no. 1, p. 79-100.

974

975 Hayashi, J., and Self, S., 1992, A comparison of pyroclastic flow and debris
976 avalanche mobility: *Journal of Geophysical Research: Solid Earth (1978–2012)*, v. 97,
977 no. B6, p. 9063-9071.

978

979 Henry, C. D., and Faulds, J. E., 2010, Ash-flow tuffs in the Nine Hill, Nevada,
980 paleovalley and implications for tectonism and volcanism of the western Great Basin,
981 USA: *Geosphere*, v. 6, no. 4, p. 339-369.
982

983 Hoke, L., and Lamb, S., 2007, Cenozoic behind-arc volcanism in the Bolivian Andes,
984 South America: implications for mantle melt generation and lithospheric structure:
985 *Journal of the Geological Society*, v. 164, no. 4, p. 795-814.
986

987 Isacks, B. L., 1988, Uplift of the central Andean plateau and bending of the Bolivian
988 orocline: *Journal of Geophysical Research: Solid Earth (1978–2012)*, v. 93, no. B4, p.
989 3211-3231.
990

991 Jordan, T., Nester, P., Blanco, N., Hoke, G., Davila, F., and Tomlinson, A., 2010,
992 Uplift of the Altiplano - Puna plateau: A view from the west: *Tectonics*, v. 29, no. 5.
993

994 Jordán, T. E., Isacks, B. L., Allmendinger, R. W., Brewer, J. A., Ramos, V. A., and
995 Ando, C. J., 1983, Andean tectonics related to geometry of subducted Nazca plate:
996 *Geological Society of America Bulletin*, v. 94, no. 3, p. 341-361.
997

998 Kay, S. M., and Coira, B. L., 2009, Shallowing and steepening subduction zones,
999 continental lithospheric loss, magmatism, and crustal flow under the Central Andean
1000 Altiplano-Puna Plateau: *Geological Society of America Memoirs*, v. 204, p. 229-259.
1001

1002 Kober, F., Ivy-Ochs, S., Schlunegger, F., Baur, H., Kubik, P., and Wieler, R., 2007,
1003 Denudation rates and a topography-driven rainfall threshold in northern Chile:

1004 multiple cosmogenic nuclide data and sediment yield budgets: *Geomorphology*, v. 83,
1005 no. 1, p. 97-120.

1006

1007 Kött, A., Gaupp, R., and Wörner, G., 1995, Miocene to Recent history of the Western
1008 Altiplano in Northern Chile revealed by lacustrine sediments of the Lauca Basin (18
1009 15' -18 40' S/69 30' -69 05' W): *Geologische Rundschau*, v. 84, no. 4, p. 770-
1010 780.

1011

1012 Lamb, S., and Davis, P., 2003, Cenozoic climate change as a possible cause for the
1013 rise of the Andes: *Nature*, v. 425, no. 6960, p. 792-797.

1014

1015 Lamb, S., and Hoke, L., 1997, Origin of the high plateau in the Central Andes,
1016 Bolivia, South America: *Tectonics*, v. 16, no. 4, p. 623-649.

1017

1018 Lamb, S., Hoke, L., Kennan, L., and Dewey, J., 1996, Cenozoic evolution of the
1019 Central Andes in Bolivia and northern Chile: SPECIAL PUBLICATION-
1020 GEOLOGICAL SOCIETY OF LONDON, v. 121, p. 237-264.

1021

1022 Lanphere, M. A., Champion, D. E., Christiansen, R. L., Izett, G. A., and Obradovich,
1023 J. D., 2002, Revised ages for tuffs of the Yellowstone Plateau volcanic field:
1024 Assignment of the Huckleberry Ridge Tuff to a new geomagnetic polarity event:
1025 *Geological Society of America Bulletin*, v. 114, no. 5, p. 559-568.

1026

1027 Ludwig, K. R., 2003, User's manual for Isoplot 3.00: a geochronological toolkit for
1028 Microsoft Excel, Kenneth R. Ludwig, v. 4.

1029

1030 Mamani, M., Wörner, G., and Sempere, T., 2010, Geochemical variations in igneous
1031 rocks of the Central Andean orocline (13 S to 18 S): Tracing crustal thickening and
1032 magma generation through time and space: Geological Society of America Bulletin,
1033 v. 122, no. 1-2, p. 162-182.

1034

1035 Martinod, J., Husson, L., Roperch, P., Guillaume, B., and Espurt, N., 2010,
1036 Horizontal subduction zones, convergence velocity and the building of the Andes:
1037 Earth and Planetary Science Letters, v. 299, no. 3, p. 299-309.

1038

1039 McQuarrie, N., Horton, B. K., Zandt, G., Beck, S., and DeCelles, P. G., 2005,
1040 Lithospheric evolution of the Andean fold–thrust belt, Bolivia, and the origin of the
1041 central Andean plateau: Tectonophysics, v. 399, no. 1, p. 15-37.

1042

1043 Montgomery, D. R., and Brandon, M. T., 2002, Topographic controls on erosion rates
1044 in tectonically active mountain ranges: Earth and Planetary Science Letters, v. 201,
1045 no. 3, p. 481-489.

1046

1047 Myers, J., 1976, Erosion surfaces and ignimbrite eruption, measures of Andean uplift
1048 in northern Peru: Geological Journal, v. 11, no. 1, p. 29-44.

1049

1050 Muñoz, N., and Charrier, R., 1996, Uplift of the western border of the Altiplano on a
1051 west-vergent thrust system, northern Chile: Journal of South American Earth
1052 Sciences, v. 9, no. 3, p. 171-181.

1053

1054 Narr, W., and Suppe, J., 1994, Kinematics of basement-involved compressive
1055 structures: *American Journal of Science*, v. 294, no. 7, p. 802-860.
1056

1057 Pinto, L., Hérail, G., and Charrier, R., 2004a, Sedimentación sintectónica asociada a
1058 las estructuras neógenas en la Precordillera de la zona de Moquella, Tarapacá (19°
1059 15'S, norte de Chile): *Revista geológica de Chile*, v. 31, no. 1, p. 19-44.
1060

1061 Ponomareva, V., Kyle, P., Melekestsev, I., Rinkleff, P., Dirksen, O., Sulerzhitsky, L.,
1062 Zaretskaia, N., and Rourke, R., 2004, The 7600 (14 C) year BP Kurile Lake caldera-
1063 forming eruption, Kamchatka, Russia: stratigraphy and field relationships: *Journal of*
1064 *Volcanology and Geothermal Research*, v. 136, no. 3, p. 199-222.
1065

1066 Roche, O., Buesch, D. C., and Valentine, G. A., 2016, Slow-moving and far-travelled
1067 dense pyroclastic flows during the Peach Spring super-eruption: *Nature*
1068 *Communications*, v. 7.
1069

1070 Salas, R., Kast, R., and Montecinos, F., Salas 1., 1966. Geología y recursos minerales
1071 del Departamento de Arica, Provincia de Tarapacá. Instituto de Investigaciones
1072 Gcológicas: *Boletín*, v. 2.
1073

1074 Schoene, B., Crowley, J. L., Condon, D. J., Schmitz, M. D., and Bowring, S. A.,
1075 2006, Reassessing the uranium decay constants for geochronology using ID-TIMS U–
1076 Pb data: *Geochimica et Cosmochimica Acta*, v. 70, no. 2, p. 426-445.
1077

1078 Smith, R. L., and Bailey, R. A., 1966, The Bandelier Tuff: a study of ash-flow
1079 eruption cycles from zoned magma chambers: *Bulletin of Volcanology*, v. 29, no. 1,
1080 p. 83-103.

1081

1082 Somoza, R., 1998, Updated azca (Farallon)—South America relative motions during
1083 the last 40 My: implications for mountain building in the central Andean region:
1084 *Journal of South American Earth Sciences*, v. 11, no. 3, p. 211-215.

1085

1086 Sparks, R.S.J., 1975, The stratigraphy and geology of the ignimbrites of Vulsini
1087 Volcano, Central Italy, *Geologische Rundschau*: v. 64, no. 1, p. 497-523.

1088

1089 Sparks, R. S. J., 1976, Grain size variations in ignimbrites and implications for the
1090 transport of pyroclastic flows: *Sedimentology*, v. 23, no. 2, p. 147-188.

1091

1092 van Zalinge, M., Sparks, R., Cooper, F., and Condon, D., 2016, Early Miocene large-
1093 volume ignimbrites of the Oxaya Formation, Central Andes: *Journal of the Geological*
1094 *Society*, p. jgs2015-2123.

1095

1096 Victor, P., Oncken, O., and Glodny, J., 2004, Uplift of the western Altiplano plateau:
1097 Evidence from the Precordillera between 20 and 21 S (northern Chile): *Tectonics*, v.
1098 23, no. 4.

1099

1100 Walker, G., Heming, R., and Wilson, C., 1980, Low-aspect ratio ignimbrites.

1101 Walker, G. P., 1983, Ignimbrite types and ignimbrite problems: *Journal of*
1102 *Volcanology and Geothermal Research*, v. 17, no. 1, p. 65-88.

1103

1104 Wendt, I., and Carl, C., 1991, The statistical distribution of the mean squared
1105 weighted deviation: *Chemical Geology: Isotope Geoscience Section*, v. 86, no. 4, p.
1106 275-285.

1107

1108 Wilson, C., 1991, Ignimbrite morphology and the effects of erosion: a New Zealand
1109 case study: *Bulletin of Volcanology*, v. 53, no. 8, p. 635-644.

1110

1111 Wilson, C. J., and Hildreth, W., 1997, The Bishop Tuff: new insights from eruptive
1112 stratigraphy: *The Journal of Geology*, v. 105, no. 4, p. 407-440.

1113

1114 Wotzlaw, J. F., Decou, A., von Eynatten, H., Wörner, G., and Frei, D., 2011, Jurassic
1115 to Palaeogene tectono - magmatic evolution of northern Chile and adjacent Bolivia
1116 from detrital zircon U - Pb geochronology and heavy mineral provenance: *Terra
1117 Nova*, v. 23, no. 6, p. 399-406.

1118

1119 Wright, J. V., Smith, A. L., and Self, S., 1980, A working terminology of pyroclastic
1120 deposits: *Journal of Volcanology and Geothermal Research*, v. 8, no. 2, p. 315-336.

1121

1122 Wörner, G., Hammerschmidt, K., Henjes-Kunst, F., Lezaun, J., and Wilke, H., 2000,
1123 Geochronology ($^{40}\text{Ar}/^{39}\text{Ar}$, K-Ar and He-exposure ages) of Cenozoic magmatic
1124 rocks from Northern Chile (18-22° S): implications for magmatism and tectonic
1125 evolution of the central Andes: *Revista geológica de Chile*, v. 27, no. 2, p. 205-240.

1126

1127 Wörner, G., Uhlig, D., Kohler, I., and Seyfried, H., 2002, Evolution of the West
1128 Andean Escarpment at 18 S (N. Chile) during the last 25 Ma: uplift, erosion and
1129 collapse through time: *Tectonophysics*, v. 345, no. 1, p. 183-198.

1130

1131 Yokoyama, S., 1974, Mode of movement and emplacement of Ito pyroclastic flow
1132 from Aira caldera, Japan: *Tokyo Kyoiku Daigaku Sci. Rep.*, v. 12, p. 17-62.

1133

1134 **Figure Captions**

1135 Figure 1. (a) Digital elevation model of the Central Andes in northern Chile indicating
1136 the different morphotectonic units from García et al. (2011). (b) Simplified geological
1137 map of northern Chile (modified from García et al., 2011). (c) Detailed geological
1138 map of the study area modified from García et al. (2004), showing the drill hole
1139 locations and the location of the Molinos section (topographic elevation indicated
1140 next to each location). The geology of Peru is not shown.

1141

1142 Figure 2. Simplified stratigraphy of the Central Depression and the Precordillera. Data
1143 compiled from: ¹van Zalinge et al., 2016; ²Wörner et al. 2000a; ³García et al., 2004;
1144 ⁴Wotzlaw et al., 2011.

1145

1146 Figure 3. SW-NE cross-section of the Western Andean Slope based upon field
1147 observations and drill core data presented in van Zalinge et al. (2016). The cross-
1148 section east of hole 9 is based on the map of García et al. (2004) and fault structures
1149 are based on observations east of the Copaquilla Basin by Muñoz and Charrier
1150 (1996). (b)-(d) Google Earth™ views and line-drawn interpretations of key structural
1151 and stratigraphic relationships. (b) Undeformed upper section of the Oxaya Formation

1152 in the northern wall of the Lluta Quebrada, Central Depression; (c) Ausipar thrust in
1153 the northern wall of the Lluta Quebrada. (d) A series of sub-vertical NW-SE trending
1154 fractures along the hinge of the Huaylillas Anticline.

1155

1156 Figure 4. North-looking view of the Huaylas Basin where the Attane Quebrada
1157 dissects the Huaylas Formation. The Huaylas Formation is covered by the late
1158 Pliocene Lauca ignimbrite and Quaternary volcanic deposits.

1159

1160 Figure 5. a) Stratigraphic column of the Huaylas Formation in hole 9, indicating
1161 sample locations for U-Pb geochronology. (b) LA-MC-ICP-MS and ID-TIMS ^{230}Th -
1162 corrected $^{206}\text{Pb}/^{238}\text{U}$ dates for hole 9. ¹Dates from sample 901 and 913 from van
1163 Zalinge et al. (2016).

1164

1165 Figure 6. (a) Present-day configuration of the Cardones ignimbrite between the
1166 Molinos section (M) and the end of the anticline (E), with the reconstructed surface of
1167 unit 1. Note that the subunits in unit 1 are indicated by different shades of grey. (b)
1168 Three reconstructions with bounding (1.2° and 1.8°) and average (1.5°) initial surface
1169 slopes plotted below the present-day configuration. Subunits within unit 1 and
1170 underlying lithologies of the Cardones ignimbrite are indicated in the reconstruction
1171 with a 1.5° surface slope. Note that the base of the Cardones ignimbrite in the line-
1172 balanced reconstructions represents the restored palaeo-topography. (c) Illustrations
1173 showing how the amount of shortening and uplift related to folding and tilting were
1174 calculated. Note that the elevation of E is fixed during folding.

1175

1176 Figure 7. Stratigraphic correlation of the Huaylas Formation in: (a) hole 9 (this study);
1177 (b) the Huaylas Basin (stratigraphy based on observations in the Attane Quebrada by
1178 García et al., 2004); (c) the Copaquilla basin, west of the Oxaya Anticline
1179 (stratigraphy based on descriptions by García et al., 2004 and García and Hérail,
1180 2005). ¹Age from Wörner et al. 2000a; ²Ages from García and Hérail, 2005; ³Age
1181 from García et al., 2004.

1182

1183 Figure 8. Schematic illustration of the development of the Western Andean Slope in
1184 northernmost Chile between >22.7 Ma and ~6 Ma. (a) Between ca. 35 and >22.7 Ma,
1185 development of a palaeo-slope was characterized by structural relief growth in the
1186 east and the creation and infilling of accommodation space in the west. (b) In the
1187 early Miocene (21.9–19.7 Ma), large-volume ignimbrites of the Oxaya Formation
1188 entirely covered the pre-existing topography, forming a planar surface with a gentle
1189 slope of $1.5 \pm 0.3^\circ$. Welding compaction was greatest where the ignimbrite was
1190 thickest (i.e. infilled valleys); creating an imprint in the topography that controlled the
1191 location of future river incision. (c) By 6 Ma, this gentle surface slope had been
1192 deformed into the Huaylillas Anticline and was incised by the Lluta River. On the
1193 eastern limb of the anticline, accommodation space (the Huaylas Basin) was created
1194 and infilled by sediments of the Huaylas Formation.

1195

1196 Figure 9. Google Earth Pro satellite image of the study area, with the outlined location
1197 of the El Diablo Formation. Note the difference in appearance of the El Diablo
1198 Formation from pale to the north and dark to the south of the Lluta Quebrada.

1199

1200 Table 1. Surface slopes of young ignimbrites and their initial surface slopes. Data
1201 points 1, 2, 4 and 7 are directly form the literature. Other data were found by
1202 overlying existing ignimbrite distribution maps on Google Earth topographic imagery,
1203 from which H/L was calculated and the mean surface slopes determined.

1204

1205 Table 2. Thickness (in metres) of unit 1 and subunits in unit 1 of the Cardones
1206 ignimbrite (modified from van Zalinge et al., 2016). Numbers in bold are
1207 reconstructed thicknesses.

1208

1209 Table 3. Results of the line balanced reconstruction, using the bounding surface
1210 slopes of 1.2° and 1.8°. ‘Hinge’ refers to the reconstructed hinge of the Huaylillas
1211 Anticline between holes 1 and 5. The elevation of the base of the Cardones ignimbrite
1212 indicates the elevation of the palaeo-topography prior to eruption of the Cardones
1213 ignimbrite. Note that this elevation is relative to that of the Molinos section (M) of
1214 which the palaeo-elevation at 21.9 Ma is unknown. The elevation of M is fixed during
1215 the line-balanced reconstructions at its present-day elevation of 900 m.

1216

Figure 1

[Click here to download Figure Fig1_maps.pdf](#)

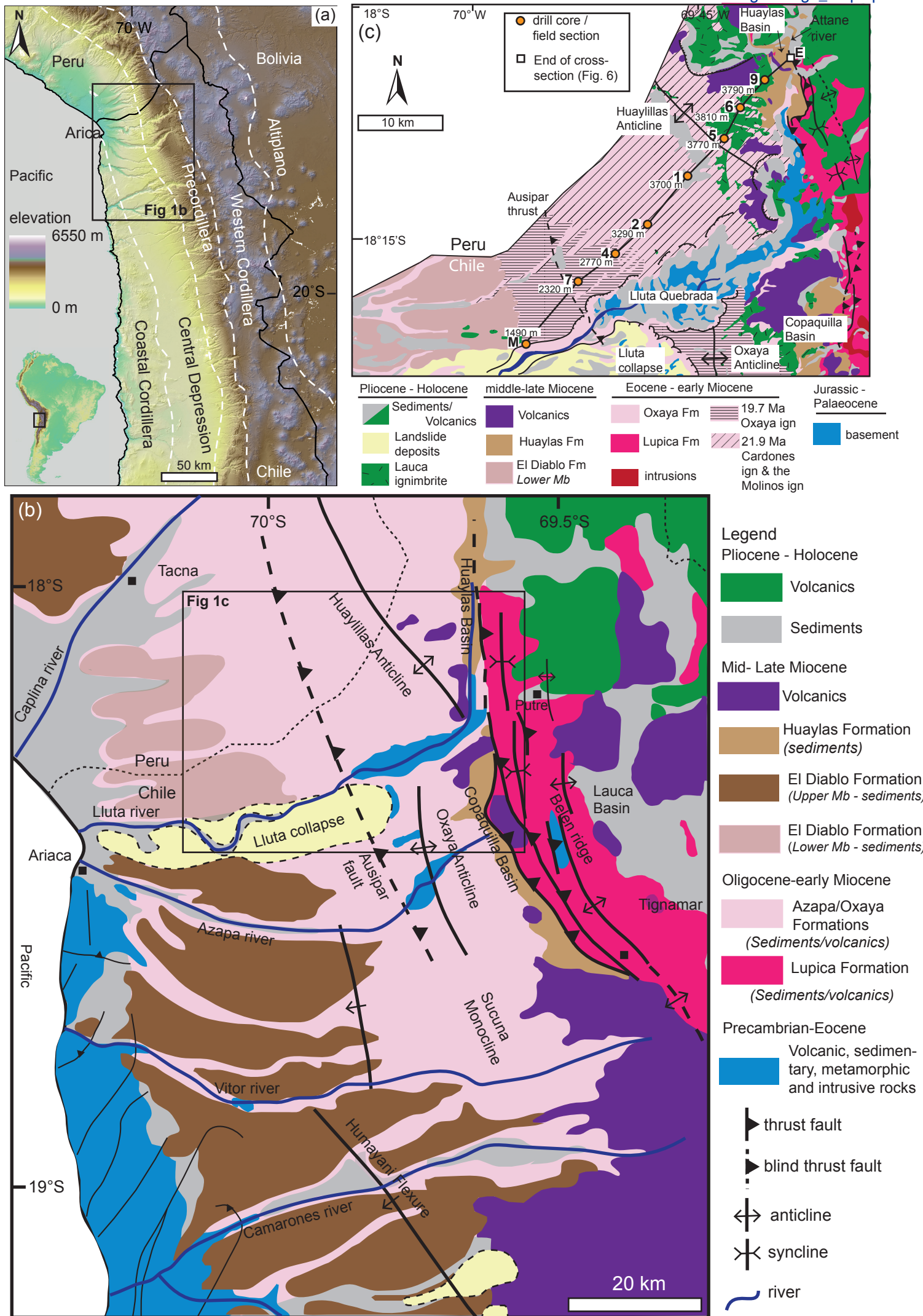


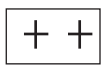
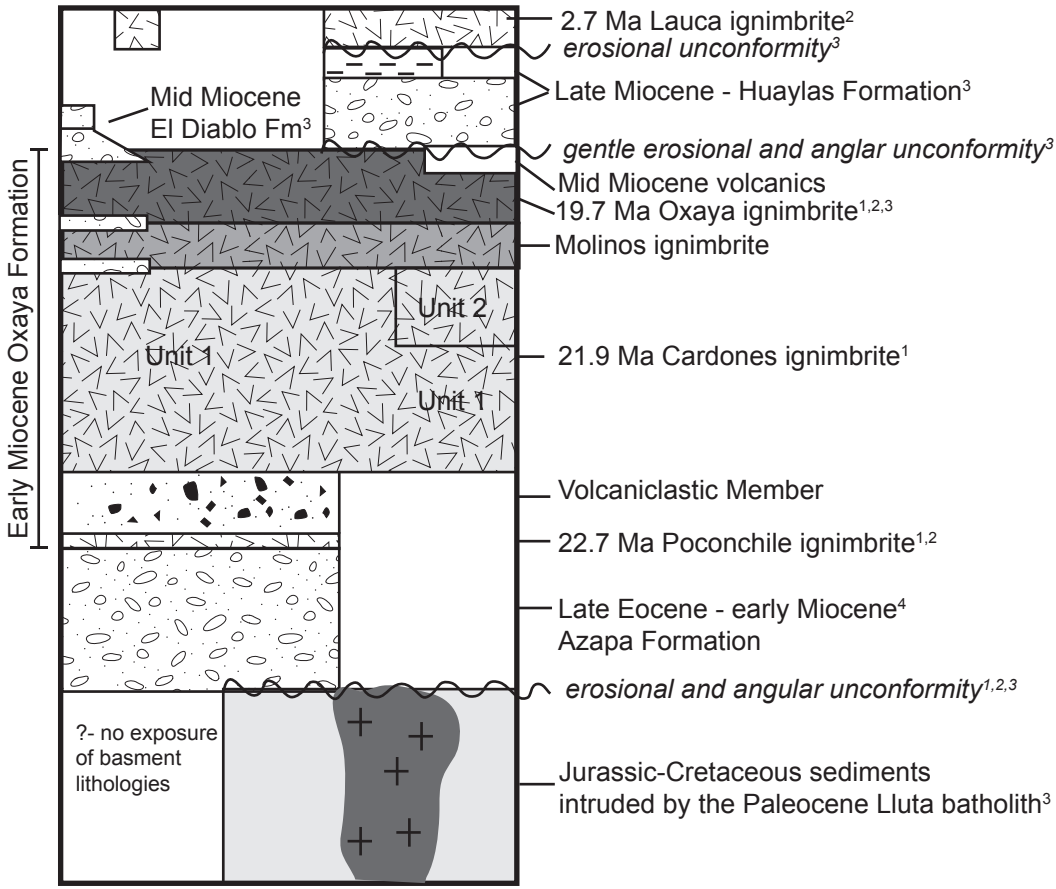
Figure 2

[Click here to download Figure 2_easystrat.pdf](#)



Central Depression

Eastern Precordillera



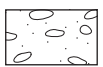
Intrusive



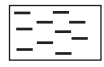
ignimbrite



volcaniclastics



coarse sandstones, gravels and conglomerates



fine lake sediments

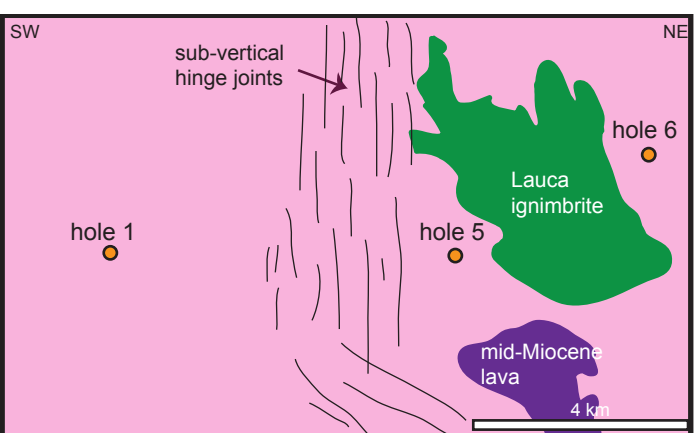
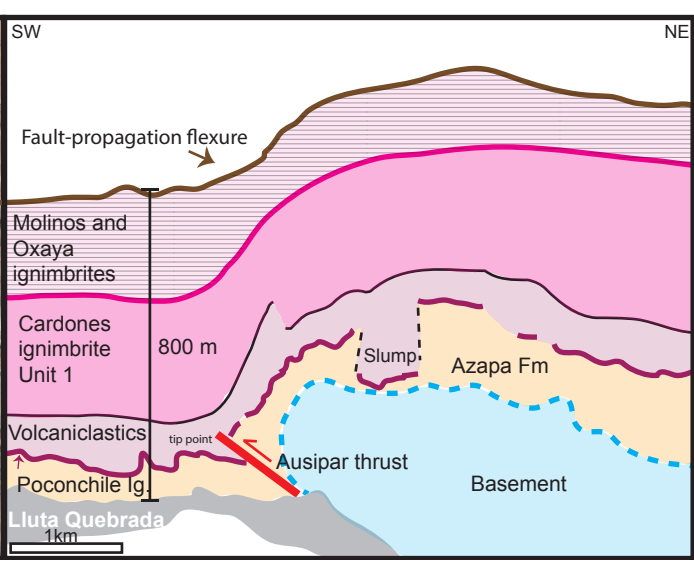
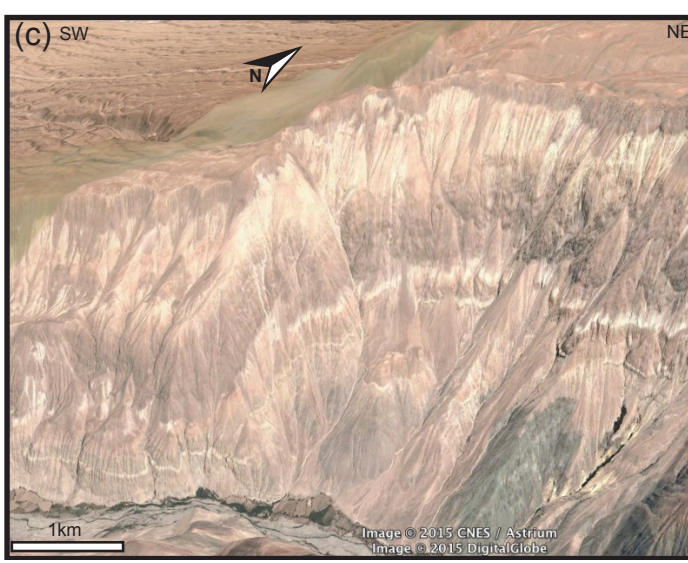
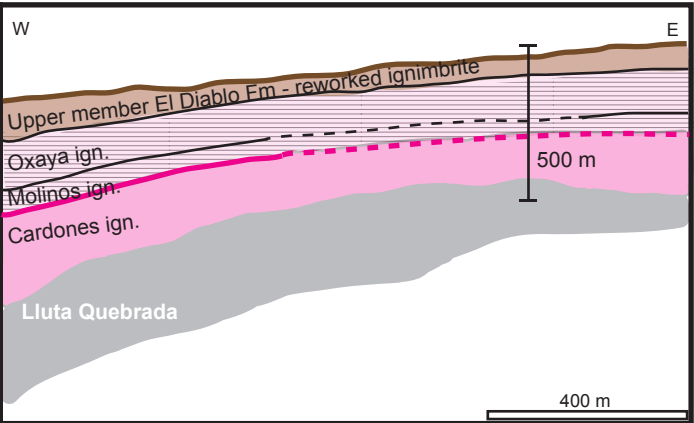
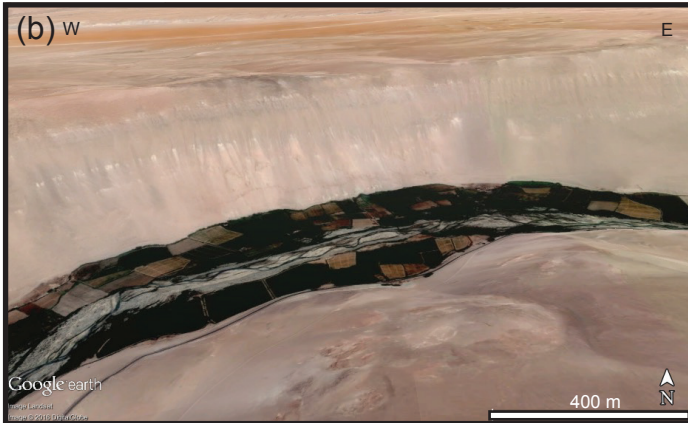
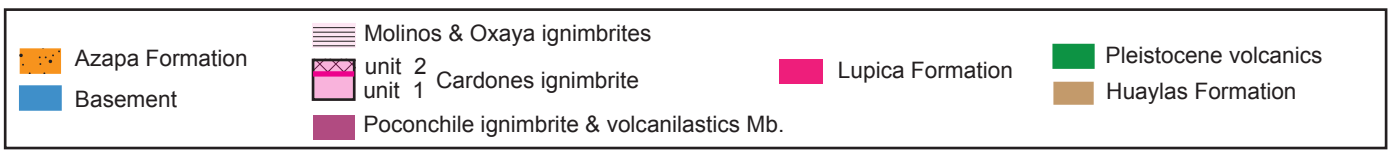
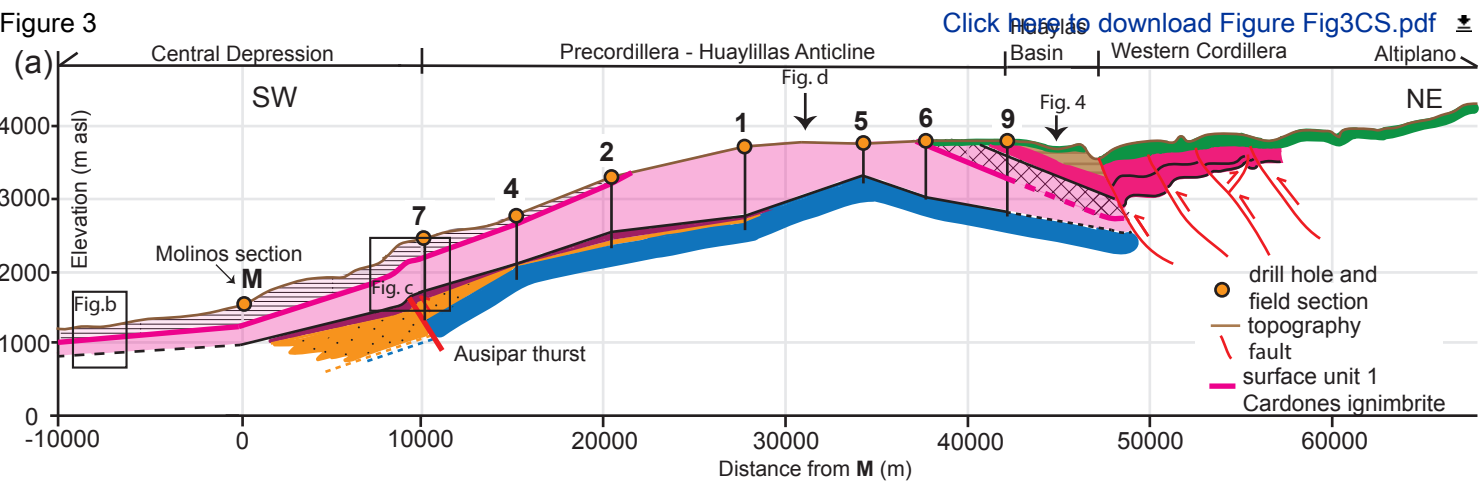


Figure 4

[Click here to download Figure Fig4.pdf](#)

Huaylas Basin

W

E

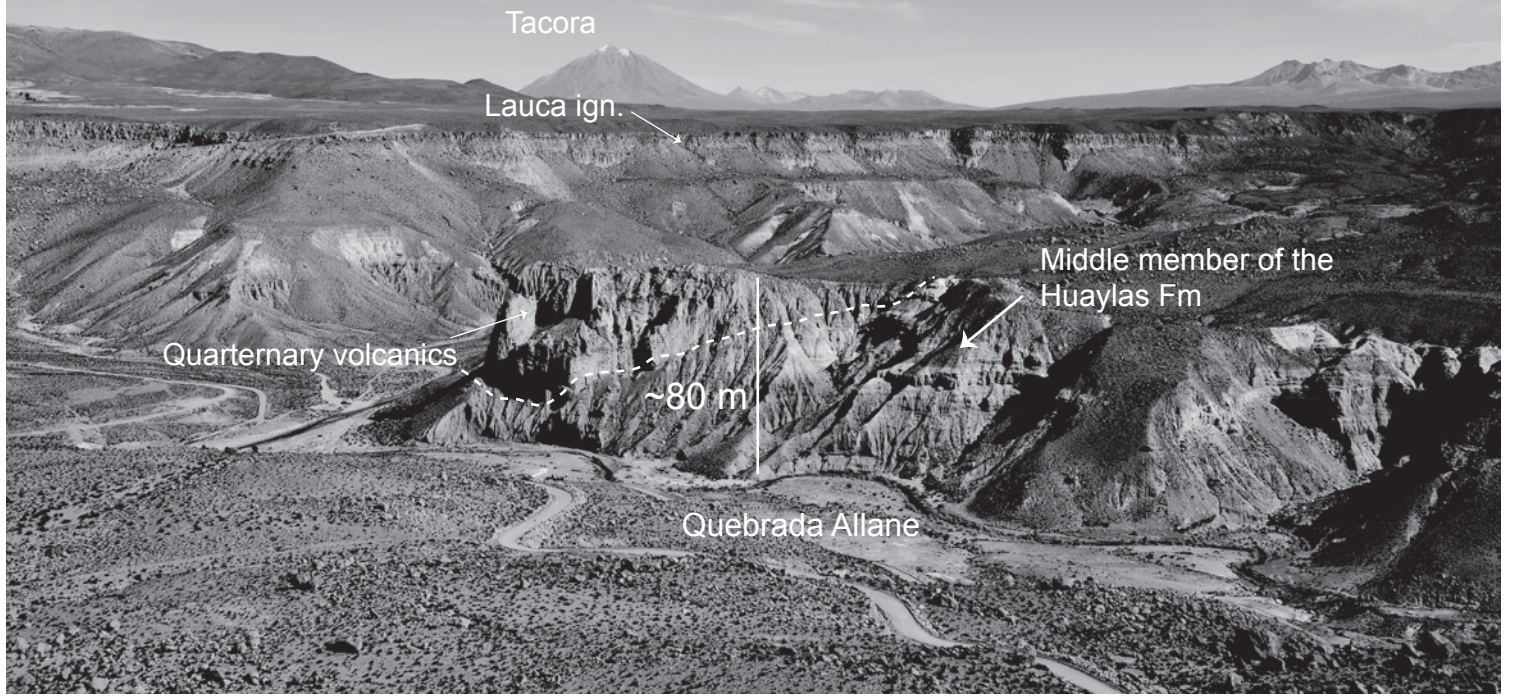
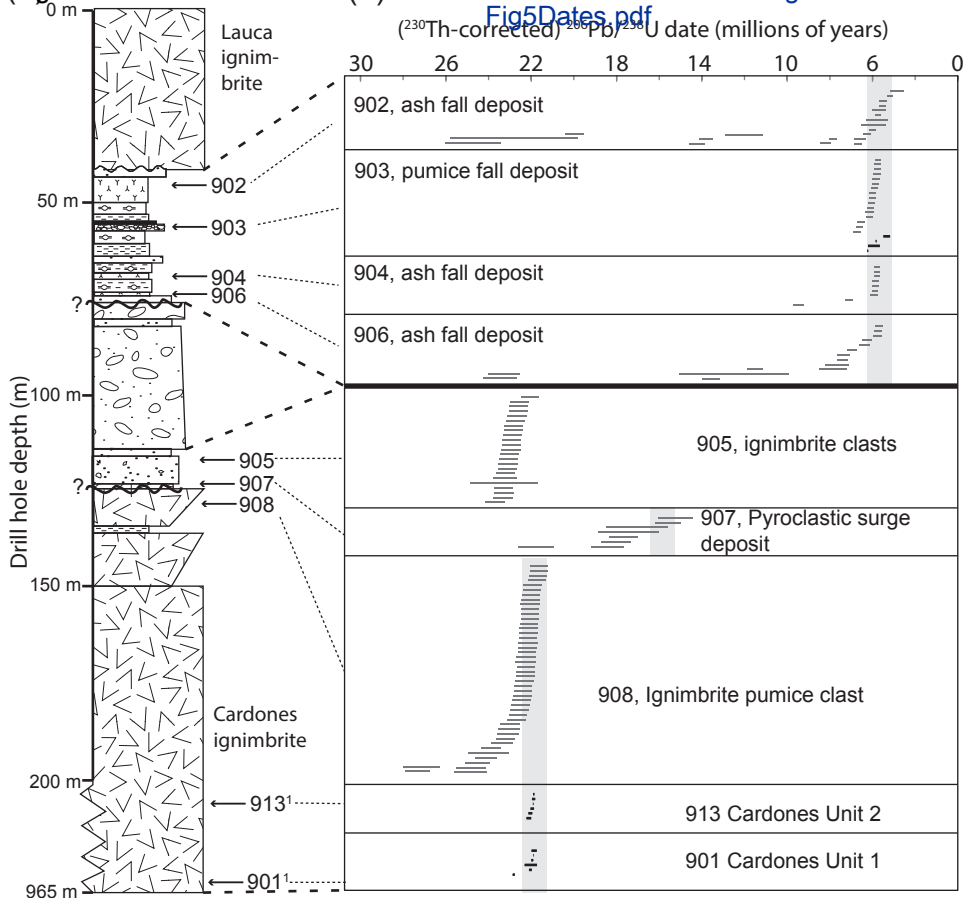


Figure 5 Hole 9

Click here to download Figure
Fig5Dates.pdf

**Key**

ignimbrite

ash fall

pumice fall

lava

diatomite

siltstone / clay

sandstone

conglomerate / gravels

peat layer

 LA-MC-ICP-MS zircon date with 2σ uncertainty

 ID-TIMS zircon date with 2σ uncertainty

Figure 6

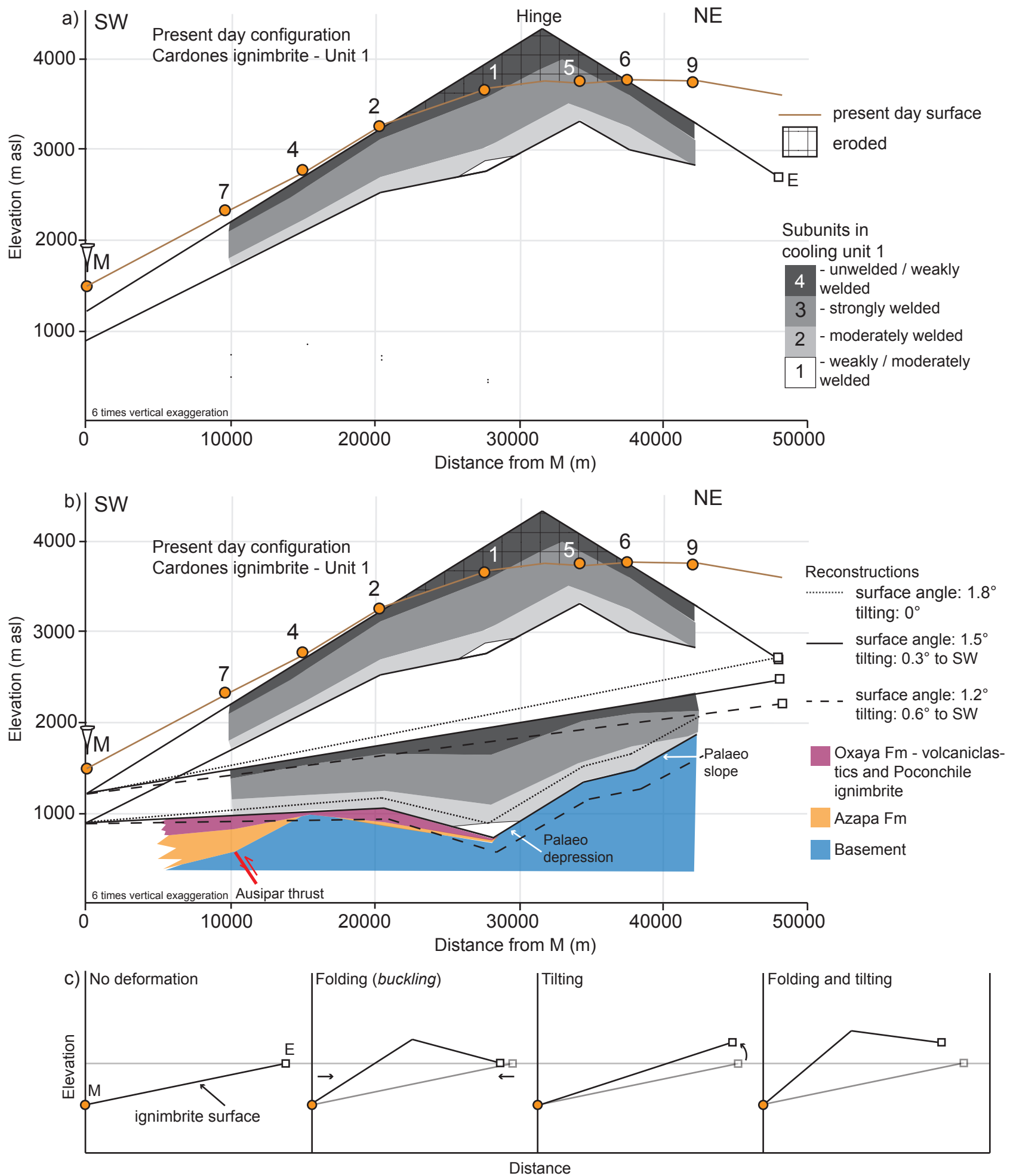


Figure 7

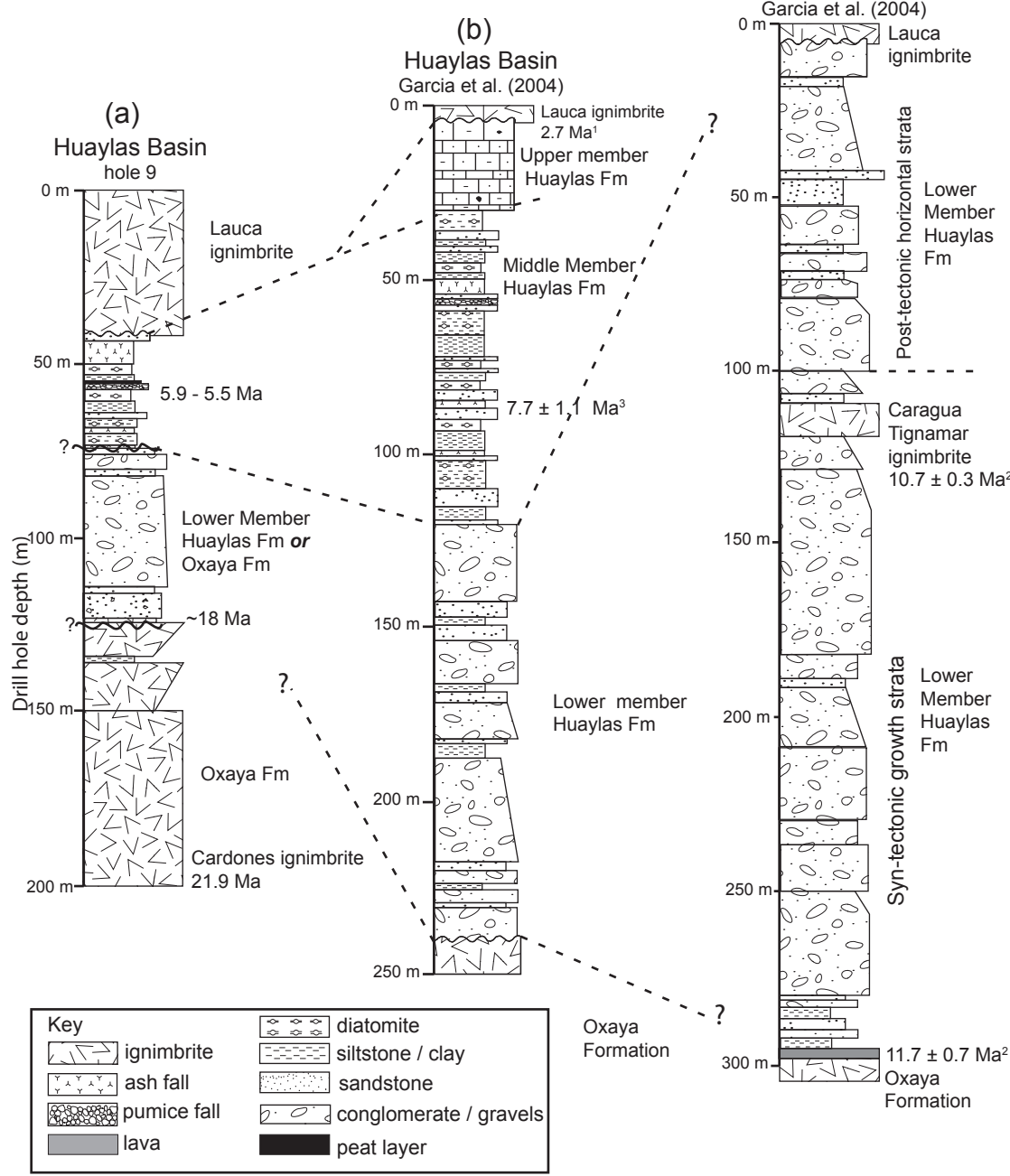
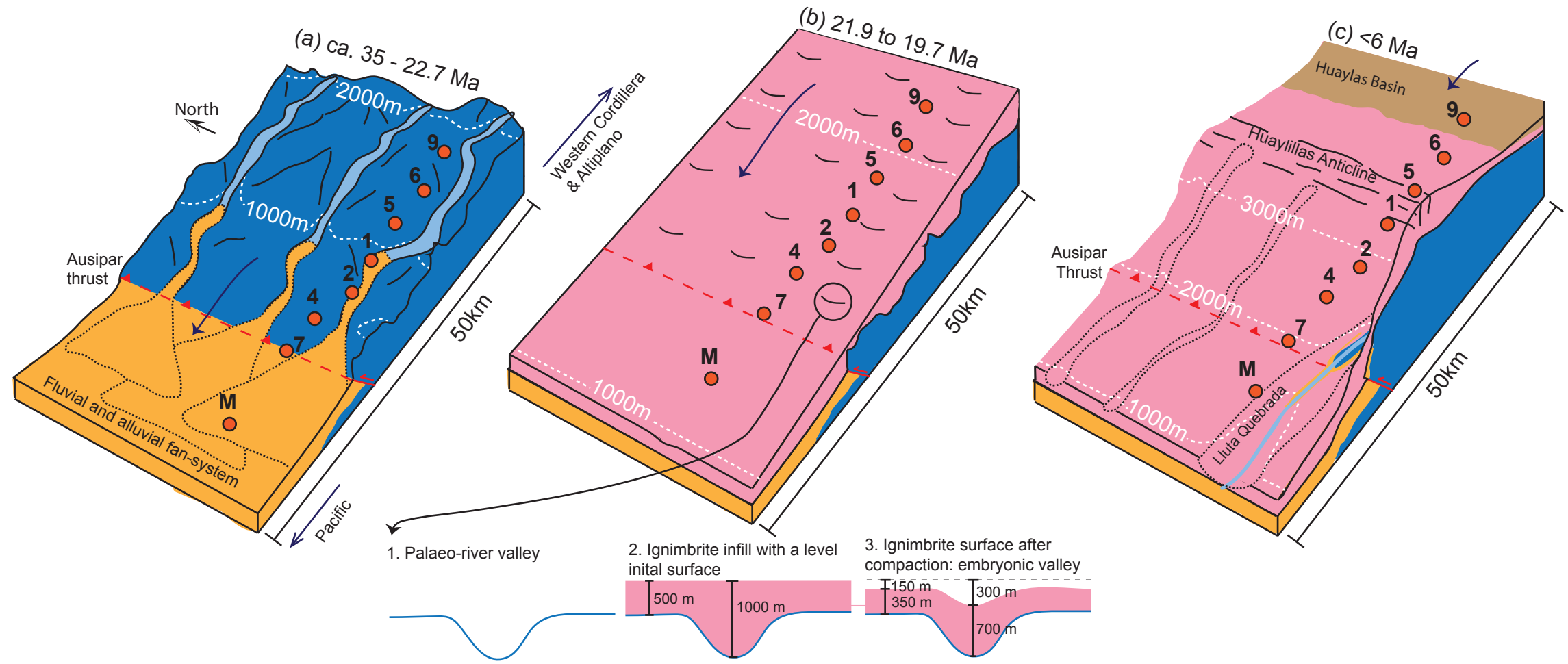


Figure 8

[Click here to download Figure Fig8Evolution.pdf](#)

● drill hole/ field section
 transport direction
 rivers
 thickest and most compacted ignimbrite creates imprint for "new" quebrada
 Basement
 Azapa Formation
 Oxaya Formation
 Huaylas Formation



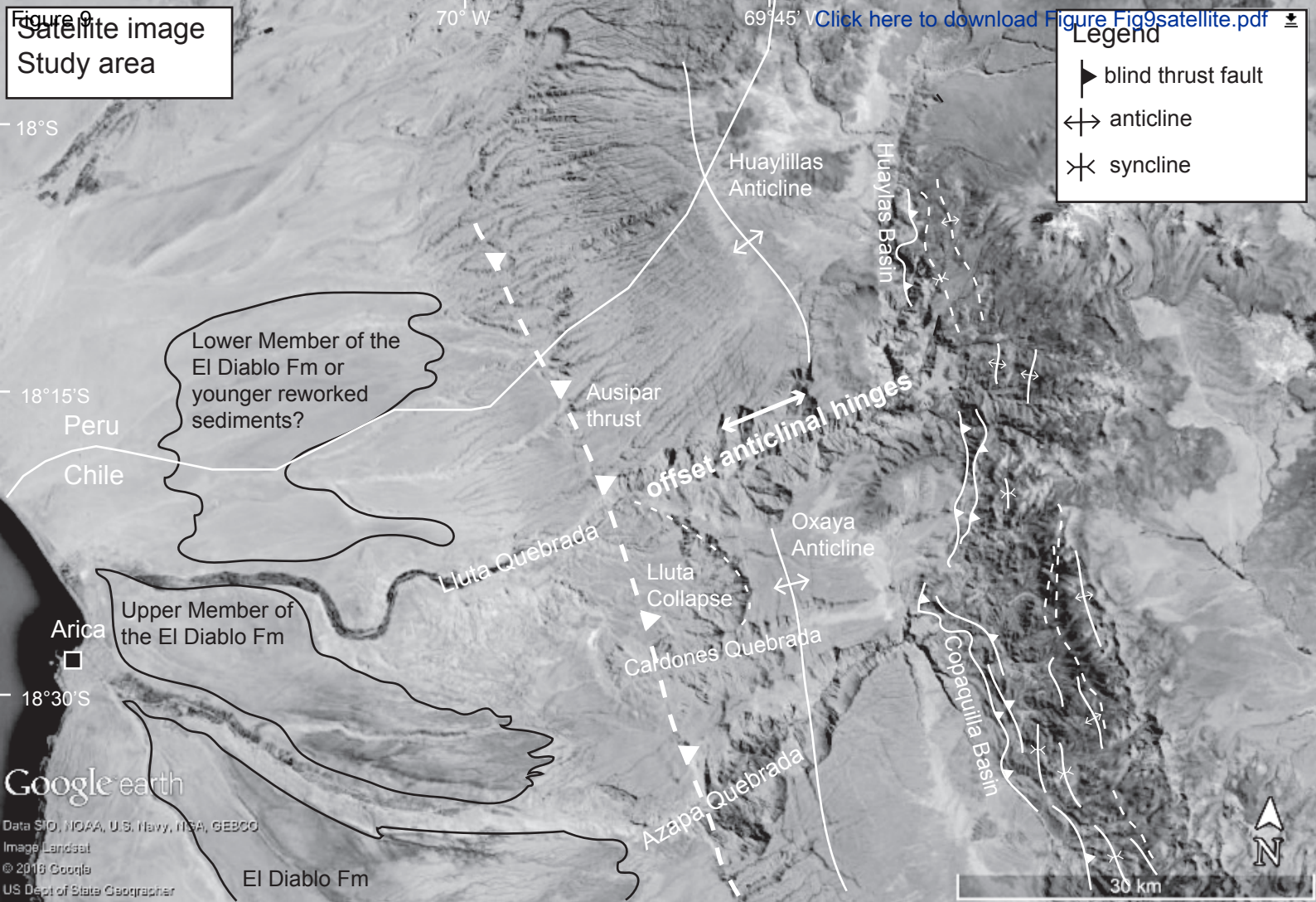


Table 1

	Deposit	Age	Average surface slope	Reference
1	The Valley of Ten Thousand Smokes ignimbrite (Alaska, USA)	1912 AD	~1.3°	Walker et al, 1980
2	Minoan Ignimbrite (Santorini, Greece)	Late Bronze age (~1650 BC)	1 - 2°	Bond and Sparks, 1976
3	Kurile-lake caldera forming ignimbrite (KO) (Kamchatka, Russia)	~7.6 kya	0.5 - 1.5°	Ponomareva et al., 2004
4	Ito-pyroclastic flow deposit (Aira Caldera, Japan)	~24.5 kya	1 - 3°	Yokoyama, 1974
5	Youngest Toba Tuff (Indonesia)	~74 kya	<1°	Aldiss and Ghazali, 1984
6	Zaragoza ignimbrite (Los Potreros Caldera, Mexico)	~100 kya	1-3°	Carrasco-Núñez and Branney, 2005
7	Bishop Tuff (Long Valley Caldera, USA)	~760 kya	1 - 5°	Wilson and Hildreth, 1997
8	Bandelier Tuff – Pajarito Plateau (Valles Caldera, USA)	~1.4 Ma	2 - 3°	Smith and Baily, 1965
9	Huckleberry ridge Tuff – Eastern Snake River Plain (USA)	~2.05 Ma	~0.5°	Lanphere et al., 2002
10	Cerro Galan ignimbrite (Argentina)	~2.08 Ma	0.5 - 2.5°	Cas et al., 2011

Table 1.

Location	Lat (S)	Long (W)	Unit 1 (m)	Sub 1 (m)	Sub 2 (m)	Sub 3 (m)	Sub 4 (m)
M	18°22'01"	69°57'14"	~300	unknown	unknown	unknown	unknown
7	18°17'59"	69°53'12"	470	0	110	250	110
4	18°16'11"	69°50'47"	580	0	150	330	100
2	18°14'15"	69°48'39"	690	0	170	410	110
1	18°11'11"	69°45'46"	1190	130	200	550	375
5	18°8'53"	69°43'01"	770	0	200	450	170
6	18°6'50"	69°42'14"	730	0	250	350	130
9	18°4'59"	69°40'32"	455	0	30	215	210

Table 3

Location	M	7	4	2	1	hinge	5	6	9	E
Ground distance from M (m)	0	9850	15240	20410	27770	31616	34200	37680	42220	48000
1.2° Surface slope – Relief growth										
Relief growth folding (m)	0	640	980	1375	1880	2140	1800	1350	755	0
Relief growth tilting (m)	0	95	150	200	275	310	340	370	415	475
Total relief growth (m)	0	735	1130	1575	2150	2450	2140	1720	1170	475
1.8° Surface slope – Relief growth										
Relief growth folding (m)	0	640	980	1375	1880	2140	1800	1350	755	0
Relief growth tilting (m)	0	-5	-10	-15	-20	-20	-20	-25	-30	-30
Total relief growth (m)	0	635	970	1360	1860	2120	1780	1325	725	-30
<i>Relief growth</i> <i>1.5° ± 0.3</i> <i>Surface slope</i>	<i>0</i>	<i>685</i> <i>±50</i>	<i>1050</i> <i>±80</i>	<i>1470</i> <i>±110</i>	<i>2005</i> <i>±145</i>	<i>2285</i> <i>±165</i>	<i>1960</i> <i>±180</i>	<i>1525</i> <i>±200</i>	<i>950</i> <i>±225</i>	<i>225</i> <i>±255</i>
Elevation of the base of the Cardones ignimbrites – Palaeo-topography pre-21.9 Ma										
<i>1.5° ± 0.3</i> <i>Surface slope</i>	<i>900</i>	<i>995</i> <i>±50</i>	<i>1025</i> <i>±80</i>	<i>1050</i> <i>±110</i>	<i>740</i> <i>±145</i>		<i>1340</i> <i>±180</i>	<i>1470</i> <i>±200</i>	<i>1860</i> <i>±225</i>	



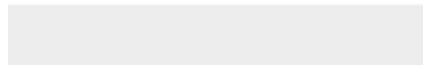
Click here to access/download
Supplemental material
Table A1.docx







Click here to access/download
Supplemental material
Table A3.xls







Click here to access/download
Supplemental material
Appendix 5.docx

